Clays and Clay Minerals, Vol. 49, No. 6, 559–585, 2001.

AUTHIGENIC PHYLLOSILICATES IN THE MIDDLE TRIASSIC KREMIKOVTSI SEDIMENTARY EXHALATIVE SIDERITE IRON FORMATION, WESTERN BALKAN, BULGARIA

ZHELYAZKO DAMYANOV[1] AND MARGARITA VASSILEVA[2]

[1] Central Laboratory of Mineralogy and Crystallography, Bulgarian Academy of Sciences, Acad. G. Bonchev St., Bl. 107, 1113 Sofia, Bulgaria

[2] Department of Economic Geology, University of Mining and Geology "St. Ivan Rilski", 1100 Sofia, Bulgaria

Abstract—Two distinct assemblages of authigenic phyllosilicates were distinguished in the Kremikovtsi sedimentary exhalative (SEDEX) siderite iron formation (SIF) and noted as important tracers of two styles of mineralization characteristic of this type of ore deposit. Hydrothermal-sedimentary layer silicates are represented by rare occurrences of relict microcrystalline Mg-rich berthierine with a relatively low degree of structural ordering, associated closely with framboidal pyrite as an intergranular matrix cementing sparry siderite grains; the larger silicates are also represented by the diagenetic transformation product of berthierine, chamosite. Berthierine precipitated under anoxic conditions during advanced early diagenesis after chert deposition. Hydrothermal-epigenetic phyllosilicates (berthierine, chamosite, illite-smectite (I-S), and kaolinite) from the barite-sulfide assemblage are characterized by: crystalline and undeformed habits; relatively larger particle size, low-temperature polytypes, low to no mixed layering, and a high degree of crystallinity; absence of impurities and dominant monomineralic aggregates; affiliation to initial open spaces and deposition mainly as vug fillings and linings. They formed under pronounced control by the vuggy porosity of the siderite host caused by the invasion of acid (pH = 3–5), hot (200–230°C) hydrothermal fluids probably at the stage of burial diagenesis of the SIF under relatively stable reducing conditions fluctuating near the sulfide/sulfate stability boundary ($\log P_{O_2} \cong -30$). The greater Al concentration in hydrothermal solution than in seawater determines the affiliation of phyllosilicates in the Phanerozoic SEDEX SIFs to aluminous species (berthierine, chamosite) unlike low to non aluminous ones (greenalite, stilpnomelane) in the Precambrian IFs. The berthierine compositions, expressed by the Mg/Fe *vs.* Al/Si ratios, are a sensitive indicator of the geological conditions under which they formed (marine, non-marine, hydrothermal ore and pre-ore), thus allowing the genetic discrimination of this mineral from various localities.

Key Words—Barite, Berthierine, Carbonate-hosted, Chamosite, Illite-smectite, Iron Formation, Kaolinite, SEDEX, Siderite.

INTRODUCTION

A generalized scheme of ore formation in the Kremikovtsi carbonate-hosted SEDEX iron (+Mn)-barite-sulfide deposit, Western Balkan, Bulgaria, based on the analysis of a vast amount of material, was presented in a previous work (Damyanov, 1998). An attempt is made in the present paper to address the phyllosilicate mineral formation in the Middle Triassic Kremikovtsi SIF—a key element to understanding the origin of the deposit.

Generally, phyllosilicates are not in great abundance in the mostly Precambrian cherty iron formations (excluding the silicate facies being of limited distribution) unlike the mostly Phanerozoic oolitic ironstones in which they are, as a rule, a major constituent (James, 1954, 1966; Maynard, 1983; Kimberley, 1989, *etc.*). The basic difference in the phyllosilicate mineralogy of iron formations and ironstones, however, is not the relative mineral abundance, but the relationship to compositionally distinct mineral species: low to non aluminous (greenalite, stilpnomelane, minnesotaite) in iron formations and aluminous (berthierine, chamosite, glauconite) in ironstones. Maynard (1983) gave a very plausible explanation of this general difference emphasizing the initial Al concentrations (whether as soluble complex compounds in solution or as a solid product/kaolinite precursor), closely related to the processes of metal differentiation, migration and deposition in a global scale during the periods of enormous iron ore accumulation.

In geology, however, the 'rules' often have exceptions. Bailey and Tyler (1960) described genetically unclear clay mineral associations in the Lake Superior iron ores dominated by a wide variety of aluminous species, and Tyler and Bailey (1961), and Bailey and Brown (1962) reported chlorites from Precambrian iron formations some of which may indeed have been diagenetic products but not induced by external agents. In contrast, Schultz (1966) noted diagenetic chlorite and rare occurrences of late diagenetic stilpnomelane and minnesotaite in the Mid–Lower Carboniferous Tynagh cherty hematite iron formation, Ireland.

In this paper we report data on authigenic phyllosilicates from the Middle Triassic Kremikovtsi SIF which seem to be unusual in light of the aforesaid: it has the main characteristics of iron formations, on the one hand, and, at the same time, is Phanerozoic in age

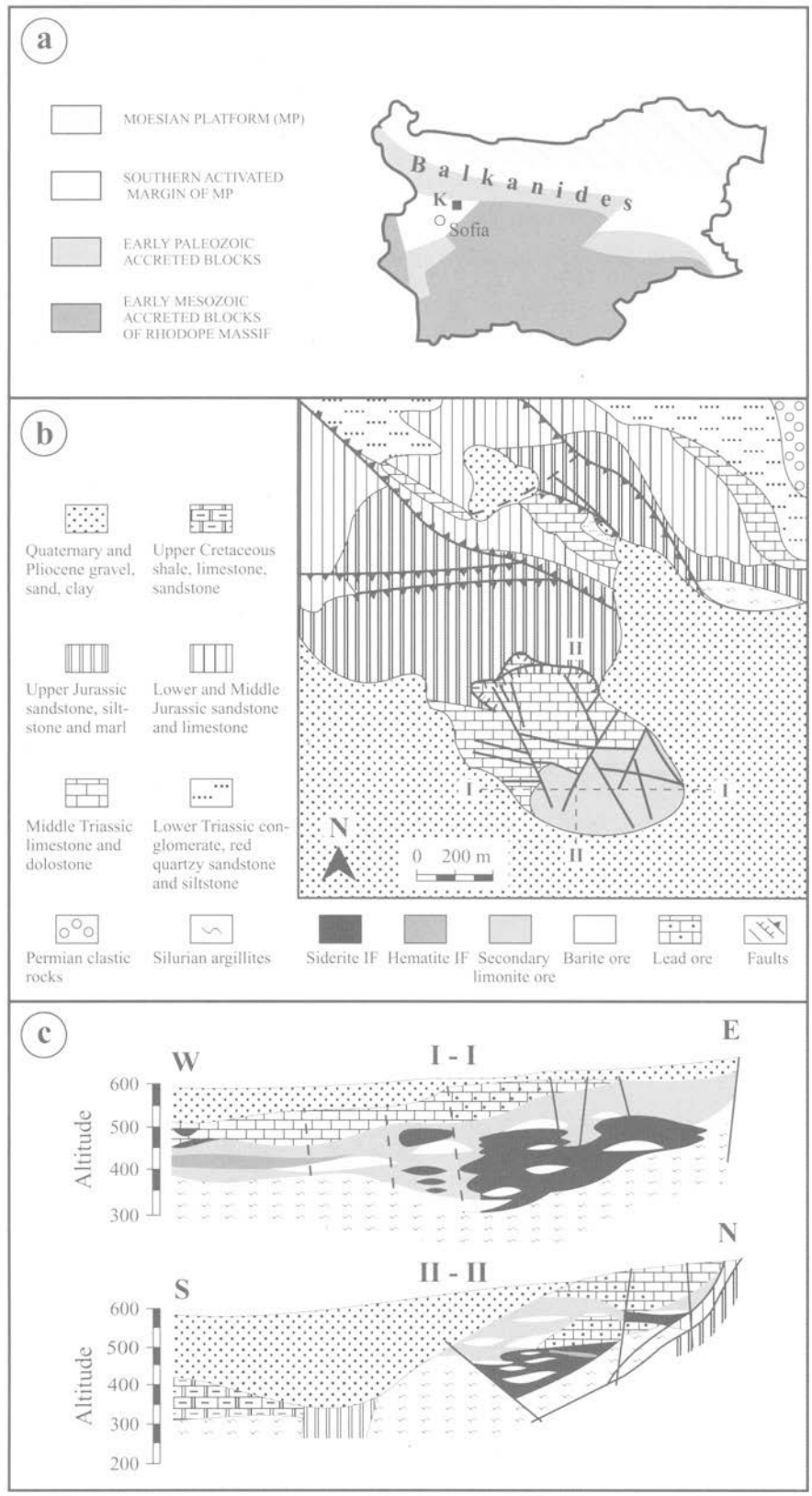

Figure 1. Tectonic sketch map of Bulgaria with elements of the accreted collage systems (a) (after Vassileff, 1993, simplified),

https://doi.org/10.1346/CCMN.2001.0490607 Published online by Cambridge University Press

and the layer silicates found (berthierine, chamosite, I-S and kaolinite) are typical of ironstones. The second important feature of this deposit with regard to its phyllosilicate mineralogy is the complicated combination of two styles of mineralization: (1) hydrothermal-sedimentary; and (2) hydrothermal-epigenetic in open spaces, both locally altered by tectonically induced low-grade dynamic metamorphism. Every one of them is characterized by its own assemblage of layer silicate minerals specified by morphology, composition and structural characteristics.

The purpose of this work was to study the features of the phyllosilicates in the Kremikovtsi SIF in order to deduce mineralogical tracers capable of identifying the processes of their formation.

GEOLOGICAL SETTING

The Kremikovtsi SIF is a constituent of the carbonate-hosted SEDEX iron (+Mn)-barite-sulfide deposit of the same name. It is located ~15 km northeast of Sofia, close to the boundary of the Sofia Trough and the Western Balkanides—a northern branch of the global Alpine-Himalayan collisional orogenic belt on the Balkan Peninsula (Figure 1a).

Mesozoic sedimentary rocks are predominant in the region (Figure 1b). Middle Triassic dolomitic limestones host the main part of the stratiform and lenticular orebodies of the Kremikovtsi SIF (Figure 1c). The geological structure is dominated by the post-Cretaceous Kremikovtsi thrust and complicated by second-order block-tectonic movements forming graben-horst-like displacements of ore bodies and by intense folding with submeridional axial direction and westward vergence.

The Kremikovtsi deposit is a large zonal carbonate-hosted SEDEX-type deposit consisting of stratiform pyrite and barite orebodies (intermediate facies), and MECS-IF-type (Metazoan-poor, extensive, chemical-sediment-rich shelf-sea iron formation) (Kimberley, 1989) siderite and hematite iron formations with low-grade stratabound sulfide mineralization (distal facies) as well as their respective stockwork and vein iron carbonate-barite-sulfide occurrences in the underlying rocks and ores (Damyanov, 1996, 1998). It was a product of polystage Middle Triassic metallogenesis located in the marginal parts of a second-order graben-shaped structure adjacent to the West Balkan early Paleozoic accreted block and related to an incipient rift setting. Location of large stratiform and lenticular siderite ore bodies in the southern and southeastern parts of the deposit and their upward transition into ankeritic ferroan dolomite, dolomitic limestone, and dolomite outline the general tendency of ore zoning (Figure 1b, c). The primary ores were produced by superimposed sedimentary and hydrothermal ore-forming processes, involving precipitation and diagenesis, fissure- and cavity-filling, and replacement. A tectonic reworking occurred either during or after the Upper Cretaceous and Tertiary collisional tectonomagmatic events, expressed mainly as two-fold thrusting of the deposit northwards.

More than 90% of the Kremikovtsi SIF is composed of siderite, quartz and barite forming three main assemblages: siderite (± ferroan dolomite and ankerite), quartz-chlorite (± berthierine and framboidal pyrite), and barite-sulfide (+ kaolinite, quartz, chamosite, I-S and berthierine) (Damyanov, 1998). The siderite is mainly fine-grained (recrystallized femicrite) with massive, rarely fine-banded, texture. Its grains are mostly cemented by microquartz (± layer silicates). Stratabound barite-sulfide (common sulfides of Fe, Pb, Zn, Cu + layer silicates) mineralization is sporadically disseminated within the SIF as pore and vug fillings, vug linings and replacements.

The geological age of the SIF, determined by dating fossil remains in the siderite ore, is contemporaneous with the host rocks and falls in a relatively limited stratigraphic interval: from the highest Lower Triassic (Spatian) to the lowest parts of the Lower Anisian (Aegean + Bithynian) Substage of the Middle Triassic (Tronkov and Damyanov, 1993).

MATERIALS AND METHODS

The several dozens of samples used in this investigation were collected from all available mining levels with siderite ore exposures in the Kremikovtsi open pit during regular field trips in the last 10 years. The mode of occurrence of phyllosilicate minerals was examined by means of transmitted and reflected light microscopy in more than 40 thin and polished sections. Routine X-ray diffraction (XRD) patterns were obtained from all samples of interest. Several representative samples of each type of phyllosilicate, according to their modes of occurrence and mineral variety, were selected for detailed analysis. Fresh pieces for scanning electron microscopy (SEM) and microprobe examinations as well as powder subsamples for XRD studies were separated from each sample.

The micromorphology, size and chemical composition of phyllosilicates were determined by employing a Philips SEM-515 with an Edax PV 9100 EDS system, operated at 30 keV (for SEM examination) as well as at 20 nA/15 keV and electron beam diameter of 0.5 μm (for microprobe analysis). The detection

←

geological map of the Kremikovtsi ore field (b), and cross-sections of the deposit (c) (after Popov, 1989, with some additions from Panayotov, 1974; Kalaydzhiev, 1982).

https://doi.org/10.1346/CCMN.2001.0490607 Published online by Cambridge University Press

limits were 0.05 wt.%. For optimal microprobe data, the analyses were performed, if possible, on particles of sufficient size. Pure natural chlorite and biotite tested by ASTIMEX Scientific Ltd were used as standards. The Fe^{2+}/Fe^{3+} = 9:1 (McDowell and Elders, 1980) and Fe^{2+}/Fe^{3+} = 1:4 (Warren and Curtis, 1989) ratios were adopted for a more realistic representation of the microprobe analyses, respectively, of chamosite and berthierine and of I-S.

A preliminary study by transmission electron microscopy (TEM) was performed on some samples prepared from an alcohol suspension of the sample powder, using a Philips EM 420T TEM with an Edax analyzer. The elemental ratios in minerals examined using analytical TEM and microprobe analysis showed a relatively good coincidence. The microprobe data were preferred as quantitatively more reliable especially; there were no facilities to prepare ion-thinned specimens or to obtain selected area electron diffraction (SAED) patterns of chemically analyzed areas. Electron diffraction patterns with 14 Å periodicity were obtained only from rosette chamosite by conventional fringe imaging.

The XRD patterns from selected samples which were prepared by the standard methods were air dried, glycolated, heated at 550°C, and treated with hot 50% HCl for 3 h, were recorded using a Dron UM-1 diffractometer employing Fe-filtered CuKα radiation, accelerating voltage of 40 keV, current of 30 mA, and scanning speed of 0.5°2θ/min. The polytype identification was carried out according to Bailey's (1988a) criteria, the relative proportions of 1*M* *vs.* $2M_1$ polytypes in I-S, according to the approach used by Maxwell and Hower (1967), and the I-S expandability—according to the conventional method compared with data calculated using the Scherrer equation (Eberl *et al.*, 1987).

PHYLLOSILICATE MINERALOGY

Phyllosilicates are minor minerals in the Kremikovtsi SIF. They comprise up to 5–6% (usually 2–3%) of the material and this correlates closely with the Al_2O_3 content of which phyllosilicates are the main bearer. In any case, however, the interest in these minerals is defined not so much by their abundance in the ore deposits as by the fact that they are very good genetic indicators of the processes and conditions under which they formed.

The main characteristics of the layer silicates from the Kremikovtsi SIF are given in Table 1. Generally, their aggregates as well as the related assemblages are disseminated within the bulk siderite without any evidence of microtectonic control of distribution.

Berthierine

Berthierine, an Fe-Al, 1:1-type layer silicate with a basal spacing of 7 Å, belonging to the serpentine subgroup, is a relatively rare mineral in the Kremikovtsi SIF. Two types of berthierine can be distinguished based on morphology: (1) microcrystalline matrix (Figure 2a); and (2) fine-grained radial blades (Figure 2b). Both types show the same textural relationship with the bulk siderite as a pore/vug-filling pale green cement of siderite grains and aggregates, but differ in the minerals with which they are associated. Microcrystalline berthierine was observed only in two samples from the relatively slightly altered parts of the Kremikovtsi SIF. It associates with a number of pyrite framboids and microquartz crystallites in a common microcrystalline matrix cementing grains or aggregates of sparry siderite (Figure 2a). Radial bladed berthierine cements coarse-grained limpid euhedral siderite (Figure 2b) as a part of fillings of the barite-sulfide assemblage. The abrupt termination of the berthierine blades at the base, as well as the lack of replacement textural relationships support formation of this morphological type as a precipitate from solution.

The XRD patterns of berthierine-dominated samples from the two types observed showed the presence of minerals typical of the assemblages in which they were included (Figure 3). Microcrystalline berthierine has a lower degree of structural ordering than the radial bladed variety as can be deduced from a comparison of randomly oriented XRD patterns (Figure 3). The relatively broader and poorly formed character of peaks of the first type and especially its diffuse 2-dimensional 020 diffraction band at 4.69 Å which suggests imperfections in the form of $\pm b/3$ layer shifts (Brindley, 1961; Nikolskaya *et al.*, 1986) support such an interpretation. As the sample containing radial bladed berthierine represented, in fact, a mixture between berthierine and kaolinite (Figure 3b) they were differentiated by: (1) different 060 reflections at 1.559 and 1.490 Å, respectively, indicating tri- and dioctahedral types of structure; (2) delineation of berthierine and kaolinite 001 and 002 peaks; (3) destruction of berthierine after treatment with hot HCl (Shilin *et al.*, 1979; Iijima and Matsumoto, 1982).

Based on the diagnostic criteria deduced by Brindley (1951), both types of berthierine present a mixture of two structural forms: trigonal (1*T*) and monoclinic (1*M*). It is difficult to make a precise evaluation of the dominant form in the samples studied but it appears that $1T \approx 1M$ in the microcrystalline berthierine unlike the radial bladed berthierine which is slightly dominated by the trigonal form. Since the Al_2O_3 content is greater in the microcrystalline variety (Table 2, Figure 4), this estimation is in accordance with the observations of Brindley (1982) and Bailey (1988b) that berthierine with large amounts of Al_2O_3 (smaller Fe contents and greater octahedral vacancies, respectively) appears to be more common in the 1*M* structural form whereas small amounts of Al_2O_3 are characteristic of the 1*T* form.

Table 1. Petrographic characteristics of phyllosilicate minerals from the Kremikovtsi SEDEX SIF.

Mineral	Aggregates: Form	Aggregates: Size, (mm)	Individual flakes: Morphology	Individual flakes: Diameter (μm)	Mineral association
			Detrital		
Degraded low-grade metamorphic mica			Irregular with elongate spines	60–150	Sparry siderite, microquartz, detrital mica
			Hydrothermal-sedimentary		
			Pore filling		
Berthierine/chamosite	Intergranular matrix	0.03–0.50	Microcrystalline to fine-bladed	2–5/10	Sparry siderite, berthierine/chamosite, framboidal/fine-grained pyrite, microquartz
			Hydrothermal-epigenetic		
			Vug filling and replacement		
Berthierine	Intergranular cement	0.03–0.50	Radial bladed	10–30	Hydrothermally recrystallized limpid sparry siderite or siderite metacrysts, chamosite, I-S, berthierine, kaolinite, short-prismatic quartz, barite, sulfides
Chamosite	Rosette or fan	0.03–20	Fan-shaped fibrous bundles, bladed	10–50	
I-(8–11%)S	Imbricate sheet	0.03–20	Scalloped with curled edges	2–10	
Kaolinite	Stacked plates	0.03–0.30	Pseudohexagonal	5–20	
			Vug lining		
Chamosite	Rosette	0.03–20	Radial bladed, equidimensional with angular or lobate edges	50–150	Euhedral limpid siderite, chamosite, I-S, prismatic quartz, barite, sulfides
I-(6–8%)S	Imbricate sheet	0.03–20	Irregular with elongate spines	10–25	
			Low-grade dynamometamorphic		
			Fracture filling		
Chamosite	Fan or rosette	0.5–50	Low-recrystallized radial bladed	10–50	Granoblastic siderite and quartz, I-S or chamosite + kaolinite, rare cataclastic barite and sulfides
I-(<5%)S	Fine-grained	0.5–100	Recrystallized subequant with stubby spines	5–30	
Kaolinite	Single or stacked plates	0.03–30	Pseudohexagonal	5–20	

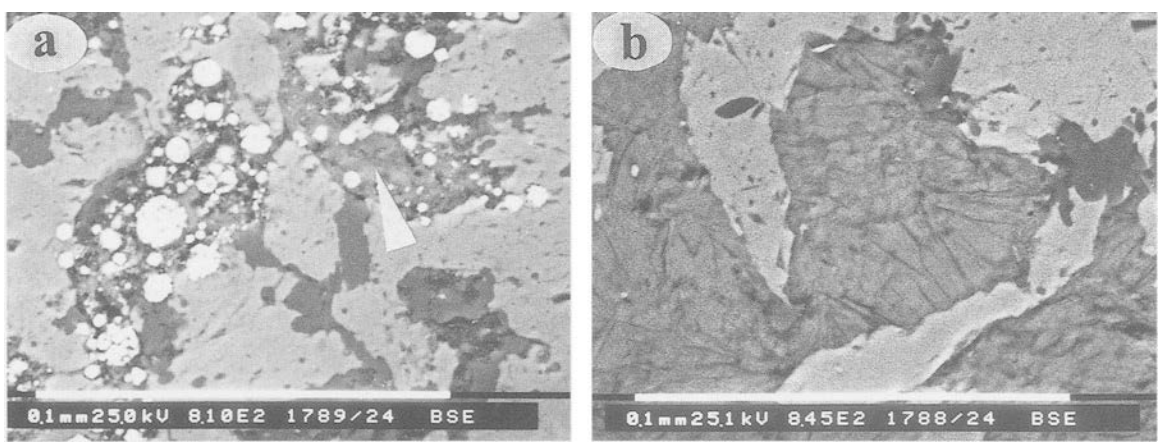

Figure 2. Back-scattered electron (BSE) photomicrographs of berthierine from the Kremikovtsi SIF. (a) Microcrystalline berthierine (arrow) associated with framboidal pyrite (white) as an intergranular matrix of sparry siderite grains (gray); microquartz (dark gray). (b) Radial bladed berthierine (gray) cementing together corroded limpid grains of hydrothermally recrystallized sparry siderite (light gray); short prismatic quartz (black).

https://doi.org/10.1346/CCMN.2001.0490607 Published online by Cambridge University Press

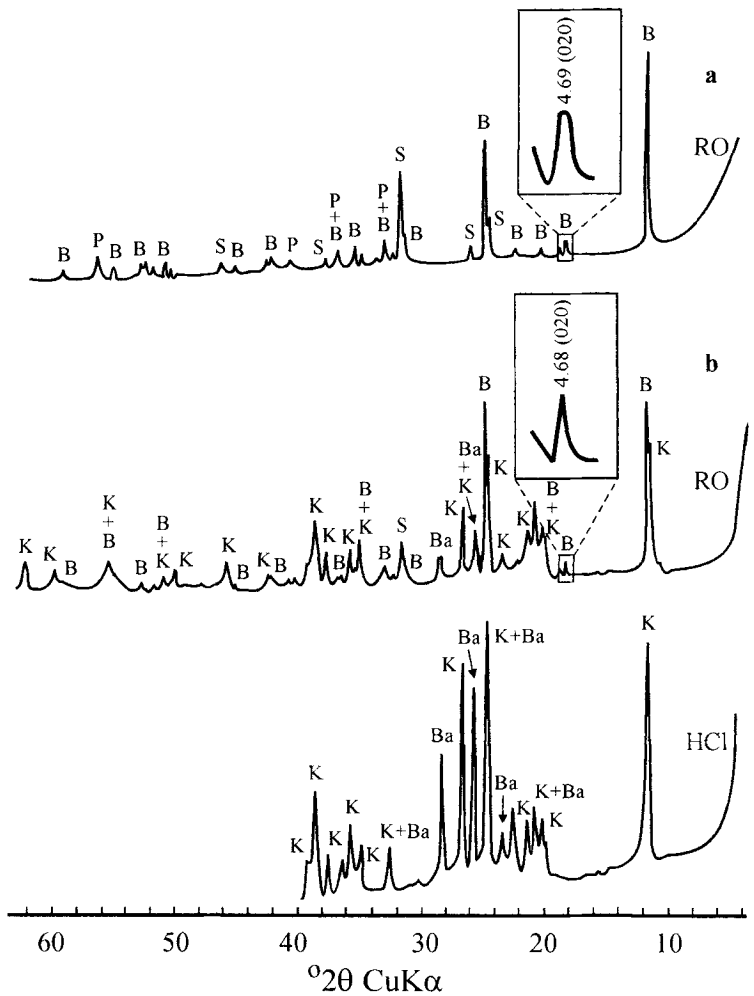

Figure 3. XRD patterns of randomly oriented (RO) and treated with hot HCl berthierine-dominated aggregate samples from the Kremikovtsi SIF. (a) Microcrystalline berthierine. (b) Radial bladed berthierine. B—berthierine; Ba—barite; K—kaolinite; P—pyrite; S—siderite; (+)—peak coincidence.

These two types of berthierine differ significantly in their chemical compositions (Table 2, Figure 4). Generally, microcrystalline berthierine has greater Al and Mg contents and more vacant octahedral positions than radial bladed berthierine which is richer in Fe and Mn. The compositional variations in the first type are greater than those in the second. The latter is also considerably more homogenous and structurally well balanced. The only common crystal chemical feature is the equal proportion (~30%) of Si substitution by Al in tetrahedral sites. The differences mentioned above determine distinct ratios and relative proportions of chemical components that are well illustrated in Figure 4. It is noteworthy that the Al content in the radial bladed berthierine is distributed equally between the tetrahedral and octahedral sites unlike the microcrystalline variety which is ^{VI}Al dominated (Figure 4c).

It is interesting that the Mg/Fe ratio in these two types of berthierine is consistent with that in the associated siderites (Damyanov, 1998), as follows: (1) Mg/Fe ≈ 0.3 for microcrystalline berthierine, and ≈0.2, for diagenetically recrystallized sparry siderite; (2) Mg/Fe ≈ 0.2 for radial bladed berthierine, and 0.1–0.2, for associated siderite metacrysts. The larger amounts of Mg in the first type of berthierine in comparison with the sparry siderite probably reflect the high Mg concentration in pore-water (trapped marine water with some hydrothermal input).

Plotting onto the diagram in Figure 4d all chemical analyses known to the authors of berthierine published in the literature, except those concerning exotic varieties such as titanian berthierine (Arima *et al.*, 1985) and zincian berthierine (Rusinova *et al.*, 1986; Slack *et al.*, 1992), the microcrystalline variety from the Kremikovtsi SIF can be defined as rich in Mg or Mg-berthierine (*cf.* Fe-berthierine reported by Toth and Fritz, 1997). The compositional field of all known berthierines is considerably larger than that given by Cur-

https://doi.org/10.1346/CCMN.2001.0490607 Published online by Cambridge University Press

Table 2. Representative microprobe analyses (wt.%) and structural formulae[1] of berthierine from the Kremikovtsi SIF.

Mode of occurrence	Pore filling						Vug filling		
Morphology	Microcrystalline						Radial bladed		
Polytype	$1T \approx 1M$						$1T > 1M$		
Sample #	K-1023/A						K-66		
SiO_2	27.20	26.76	26.25	24.35	25.95	24.84	24.58	24.14	24.43
Al_2O_3	23.45	24.27	24.73	23.50	24.23	24.53	18.41	18.69	18.86
FeO	32.28	31.11	34.44	34.36	33.16	34.00	41.96	42.18	42.09
MnO	n.d.[2]	0.01	0.41	0.31	0.16	0.33	0.55	0.68	0.59
MgO	4.85	5.21	6.60	5.65	6.32	6.08	4.48	4.26	4.07
Na_2O	0.14	0.47	0.52	0.15	0.30	0.30	n.d.	n.d.	n.d.
K_2O	0.11	0.15	n.d.	n.d.	n.d.	n.d.	n.d.	n.d.	n.d.
Total	88.03	87.98	92.95	88.32	90.12	90.08	89.98	89.95	90.04
Si	1.461	1.432	1.354	1.333	1.373	1.326	1.388	1.368	1.379
^{IV}Al	0.539	0.568	0.646	0.667	0.627	0.674	0.612	0.632	0.621
^{VI}Al	0.946	0.963	0.857	0.850	0.884	0.870	0.614	0.616	0.634
Fe	1.450	1.393	1.486	1.574	1.467	1.518	1.982	1.999	1.987
Mn	n.d.	0.001	0.018	0.014	0.007	0.015	0.026	0.033	0.028
Mg	0.388	0.416	0.507	0.461	0.498	0.484	0.377	0.360	0.343
Σ Oct	2.784	2.773	2.868	2.899	2.856	2.887	2.999	3.008	2.992
Oct vacancy	0.216	0.227	0.132	0.101	0.144	0.113	0.001	−0.008	0.008
Na	0.015	0.049	0.052	0.016	0.031	0.031	n.d.	n.d.	n.d.
K	0.008	0.010	n.d.	n.d.	n.d.	n.d.	n.d.	n.d.	n.d.
Fe/(Fe + Mg)	0.789	0.770	0.746	0.773	0.747	0.758	0.840	0.847	0.853
Mg/Fe	0.268	0.299	0.341	0.293	0.339	0.319	0.190	0.180	0.173
Al/Si	1.016	1.069	1.110	1.138	1.100	1.164	0.883	0.912	0.910
Al/(Al + Si)	0.504	0.516	0.526	0.532	0.524	0.538	0.469	0.477	0.476
Fe/(Al + Si + Fe)	0.330	0.320	0.342	0.356	0.337	0.346	0.431	0.433	0.430

[1] Formulae calculated on the basis of Σ + charge = 14.00; total Fe as FeO.
[2] n.d. = not detected.

tis *et al.* (1985) for authigenic chlorites (Figure 4d) even if the hydrothermal varieties are ignored.

Comparison with berthierines from various other locations shows that the microcrystalline variety is characteristically aluminous and Fe-poor (Figure 4b) unlike the radial bladed berthierine which is rich in bivalent cations (Figure 4a). Genetically, the first type falls into the field of marine berthierines which comprises most of the occurrences in this study (mainly in ironstones) whereas the second type tends to the 'pre-ore' varieties (berthierines from zones of low-temperature hydrothermal alteration—Rusinova *et al.*, 1986; see explanations related to Figure 15) (Figure 4a, b).

Chamosite

Chamosite, an Fe^{2+}-dominant, 2:1-type layer silicate with a basal spacing of 14 Å, belonging to the subgroup of trioctahedral chlorite, is the most widespread phyllosilicate mineral in the Kremikovtsi SIF. Several types of chamosite were observed, based on morphology and mode of occurrence: (1) replacements of siderite grains by fan-shaped fibrous bundles (Figure 5a); (2) vug fillings of bladed chamosite commonly associated with minerals from the barite-sulfide assemblage (Figure 5c, d) and rarely as monomineralic aggregates (Figure 5b); (3) vug linings of well formed rosettes overgrowing euhedral limpid siderite or barite crystals (Figure 6a–c); (4) fracture fillings of slightly recrystallized radial bladed chamosite in tectonically deformed zones (Figure 5e). The close spatial association of chamosite replacements, vug fillings and vug linings in the samples studied allows us to distinguish them using their distinct modes of deposition of building materials. This conclusion is also supported by their similar chemical compositions (Table 3; Figure 4).

A part of the so-called vug-filling chamosite that is not associated with the barite-sulfide assemblage resembles intergranular fillings characteristic of microcrystalline berthierine, implying that it was a transformation product after berthierine during progressive diagenesis. This is also proven by their compositional similarity as well as by the recrystallization of associated pyrite framboids into very fine subhedral to euhedral pyrite crystals.

The XRD patterns of chamosite rosettes and fracture fillings (Figure 7) showed the presence of well crystallized single chamosite phases but not a mixture with berthierine in significant amounts. This identification was supported by the increase of 14 Å reflection intensities on heating (Brindley, 1961; Shilin *et al.*, 1979; Nemecz, 1981).

Using the measured $d(001)$ values we can estimate the formation temperatures of chamosites based on the method proposed by Battaglia (1999): (1) 14.20 Å corresponds to 179°C (according to the regression line equation of type: $d_{001}{}^{M} = -0.001T_M + 14.379$, where $d_{001}{}^{M}$ is the measured d_{001} value, and T_M the measured in-hole geothermometric temperatures) and ~210°C

https://doi.org/10.1346/CCMN.2001.0490607 Published online by Cambridge University Press

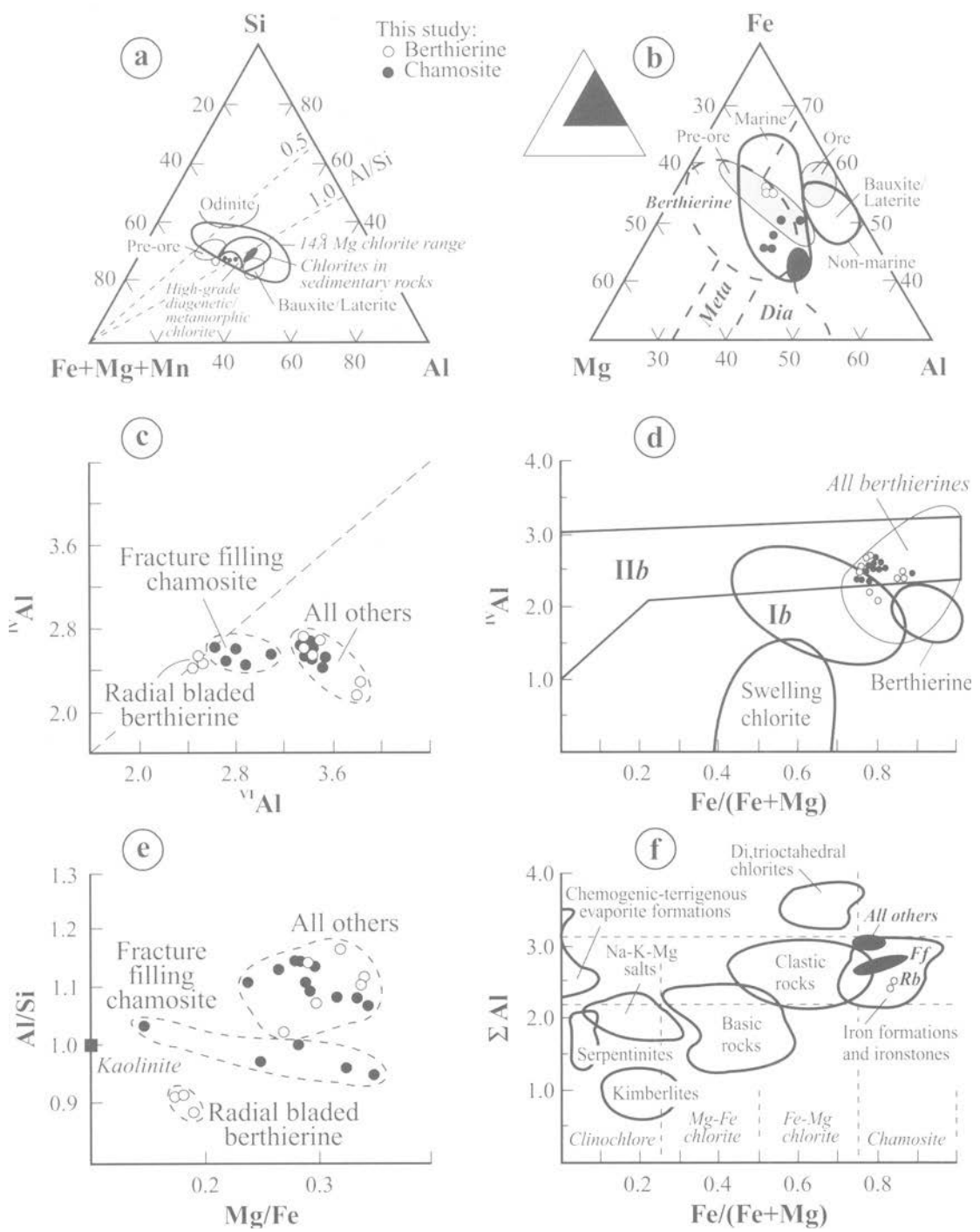

Figure 4. Chemical compositions (on the basis of 28 oxygens) of berthierine and chamosite from the Kremikovtsi SIF plotted on: (a, b) R^{2+}-Al-Si and Mg-Al-Fe triangle diagrams of chlorite compositional fields (after Velde, 1985; italicized captions). Fields of berthierine (shaded, with normal captions) based on 102 analyses (see references in Figure 15) are also shown. The field for chlorite in sedimentary rocks given on the R^{2+}-Al-Si plot includes the maximum concentration (>85%) of berthierine compositions. Data for microcrystalline berthierine are located within the large black fields of hydrothermal chamosite. Scattered solid circles indicate fracture-filling chamosite. (c, e) ^{VI}Al *vs.* ^{IV}Al and Mg/Fe *vs.* Al/Si diagrams; (d) Fe/(Fe+Mg) *vs.* ^{IV}Al diagram of different chlorite varieties (after Hayes, 1970; Curtis *et al.*, 1985). The field for berthierines, based on 102 published analyses, is also shown. (f) Fe/(Fe+Mg) *vs.* ΣAl diagnostic diagram for Mg-Fe chlorites of different origins (after Drits and Kossowskaya, 1991). *Rb*—radial bladed berthierine; *Ff*—fracture-filling chamosite.

https://doi.org/10.1346/CCMN.2001.0490607 Published online by Cambridge University Press

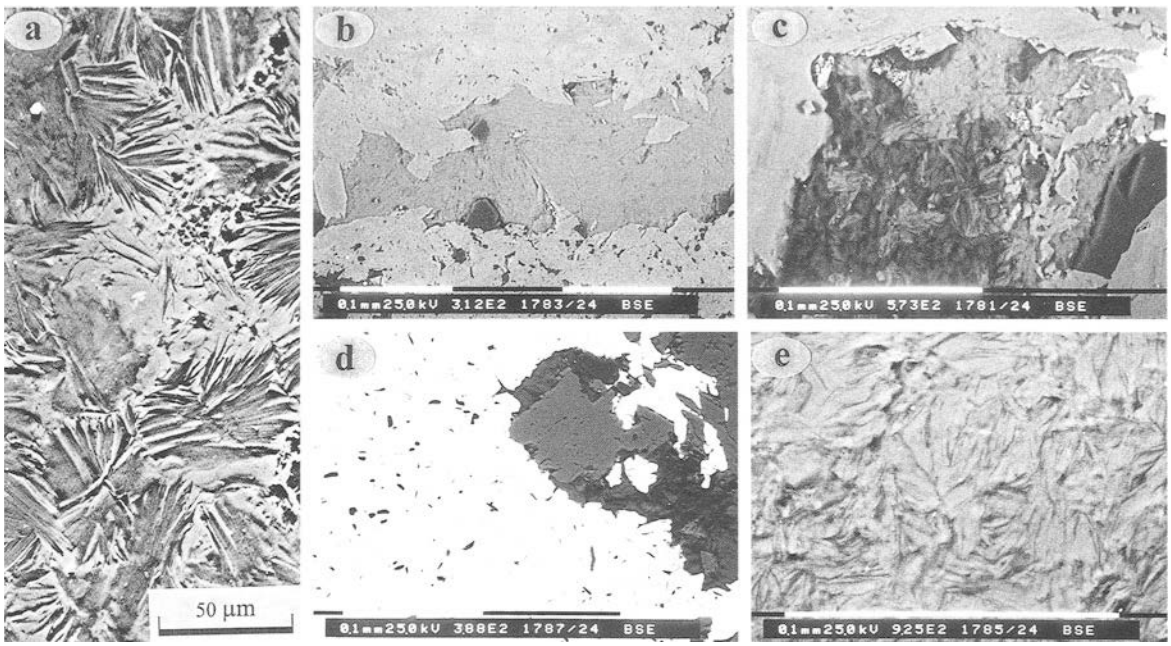

Figure 5. BSE photomicrographs of chamosite from the Kremikovtsi SIF. (a) Fan-shaped fibrous bundles of chamosite (gray) replacing sparry siderite grains (light gray). (b) Bladed chamosite (gray) filling vugs within siderite aggregates (light gray); short-prismatic quartz (black). Note the coarse-grained euhedral limpid siderite crystals on the vug walls formed as a result of hydrothermally induced recrystallization of the sparry siderite matrix. (c) Bladed chamosite (gray) associated with I-S (dark-gray), prismatic quartz (black), and barite+chalcopyrite (white) as a vug filling within siderite aggregates (light-gray); (d) Chamosite (dark-gray) replacing a euhedral limpid siderite grain (gray) within barite (white) with kaolinite inclusions (black); (e) Radial bladed chamosite filling fractures in tectonically deformed zones.

(according to the compositionally similar sample TD 2 from the Tendaho active geothermal field in the Afar rift, Ethiopia), for rosette chamosite; (2) 14.10 Å corresponds to 279°C, for fracture-filling chamosite. The first value corresponds to the temperature of homogenization of gas-liquid inclusions of the associated barite which we measured (215 ± 15°C) and the second implies the beginning of the lowest temperature anchimetamorphic alterations induced by local tectonic events.

Based on the diagnostic criteria deduced by Bailey (1988a), replacement, vug-filling, and vug-lining chamosites from the Kremikovtsi SIF belong to the *Ibb*(β = 90°) structural group (*Ib* according to Brown and Bailey, 1963, or subfamily D according to Weiss and Durovic, 1983). As is known (Walker, 1989, 1993), *Ib*(β = 90°) is the dominant chlorite group in iron formations and hydrothermal veins (although the Kremikovtsi SIF is a typical iron formation, the hydrothermal input depositing layer silicates in the barite-sulfide assemblage is obvious), and also forms preferentially in rock types that afford open space suitable for crystallization of the mineral. Thus, the dominant *Ibb*(β = 90°) group of the Kremikovtsi hydrothermal chamosite appearing as vug fillings, vug linings and rarely as replacements formed under relatively low-temperature conditions confirms Walker's (1989) observations. This is common in monostage hydrothermal vein systems. In complex multistage systems, forming, *e.g.* epithermal veins (Rusinova and Rusinov, 1980; Rusinova *et al.*, 1986) or carbonate-hosted barite-polymetallic deposits (Zhabin *et al.*, 1987), chlorites of all four structural groups were found. Those authors suggested that the diversity of modes of formation and multiple mineral deposition were possible causes of this.

Fracture-filling chamosite refers to a *IIbb*(β = 97°) group (subfamily C) that is reasonable as it recrystallized under high P-T conditions induced by post-mineral tectonic events.

Crystallochemically, chamosite from the Kremikovtsi SIF is characterized by two populations of data (Figure 4): the first one, including replacement, vug-filling, and vug-lining varieties (named for the sake of brevity 'hydrothermal' or relatively low-temperature), and the second one, including fracture fillings ('metagenetic' or high-temperature). Generally, hydrothermal chamosite differs in having smaller Fe contents and fewer bivalent cations (greater ^{VI}Al and total Al, respectively) and a lower octahedral occupancy in comparison with metagenetic chamosite which is structurally well balanced (very similar amounts of ^{IV}Al and ^{VI}Al) but much more variable chemically. It is interesting that both hydrothermal chamosite and micro-

https://doi.org/10.1346/CCMN.2001.0490607 Published online by Cambridge University Press

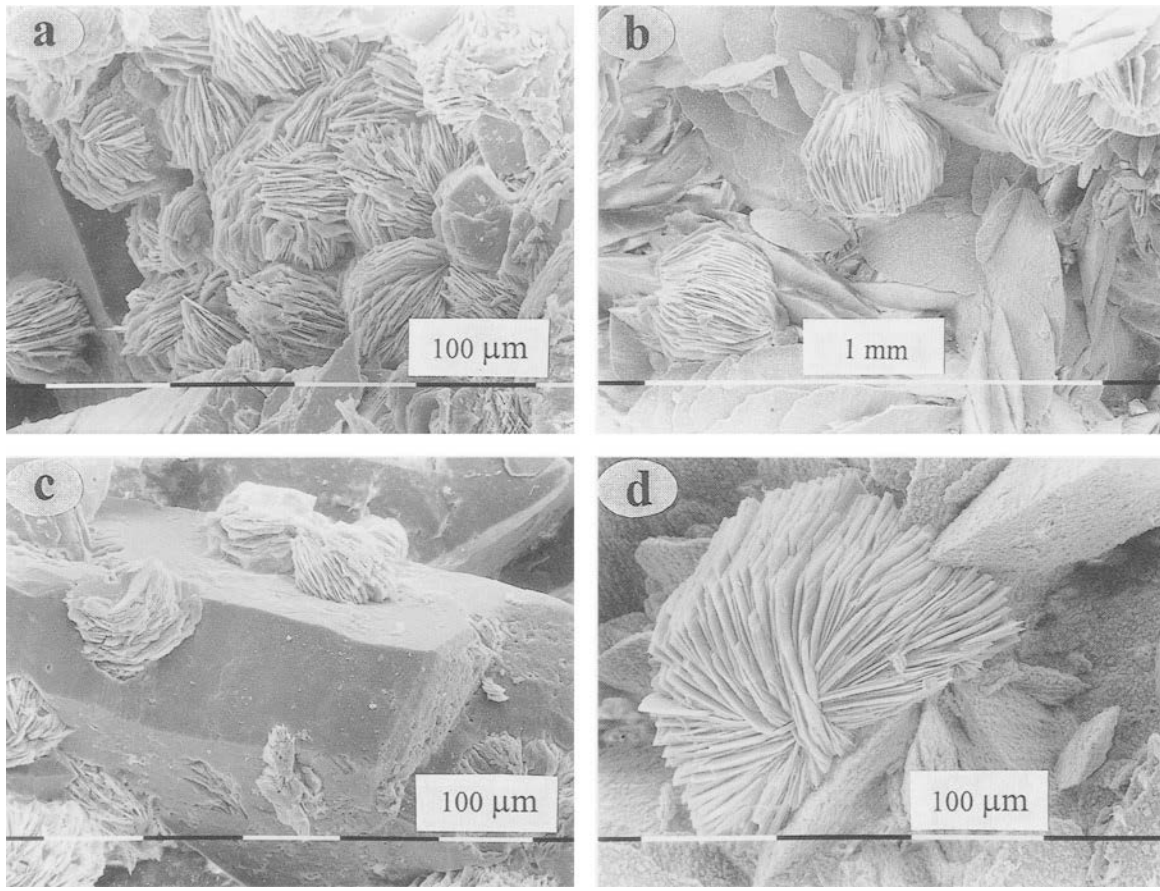

Figure 6. Secondary electron (SE) photomicrographs of vug-lining chamosite from the Kremikovtsi SIF. (a, b, d) Rosettes of radial bladed equidimensional chamosite overgrown on flattened rhombohedral grains of euhedral limpid siderite. (c) Rosettes of chamosite overgrown on barite crystals. Note that the chamosite growth started before the barite crystal growth finished, thus implying a period of synchronous common growth.

crystalline berthierine fall into common fields on all the discrimination diagrams given in Figure 4. The most plausible explanations of this fact may be: (1) the relatively uniform load of hydrothermal solution, proposed in an earlier paper (Damyanov, 1998), as entrapped in pore-water during diagenesis of hydrothermal precipitates or as deposited in solution cavities within the partially lithified SIF; and/or (2) a part of this chamosite is, in fact, a late diagenetic transformation product of microcrystalline berthierine.

Chemically, both types of chamosite lie near the boundary between the fields of *Ib* and *IIb* chlorite groups (Figure 4d) and so discrimination between them on this basis is difficult. They are well differentiated, however, on the next diagram (Figure 4f) falling entirely within the field of chlorite typical of iron formations and ironstones. The only serious compositional difference between the Kremikovtsi chamosites and chlorites in iron formations (data summarized by Albee, 1962) is the Mn content which is an average of 10 (up to 40) times greater than the upper limit given by this author. The large Mn content reflects the chemistry of the host siderite and hydrothermal solution in the Kremikovtsi ore-forming system.

Illite-smectite

Micaceous material in the bulk siderite is rare. It is represented by single flakes of detrital mica disseminated sporadically in the siderite matrix. As a rule, these clay particles were not altered during diagenesis, but fine-scale incoherent (*i.e.* not in structural continuity, White *et al.*, 1985) intergrowths between initial mica and replacing chamosite (Figure 8a) were observed in samples from zones abundant in barite and sulfides. On the basis of chemical composition and petrographic observations (Table 4; Figures 9 and 10), this detrital material can be defined as degraded low-grade metamorphic mica (illite) from surrounding late Paleozoic rocks, deposited simultaneously with siderite precipitation. Generally, the detrital supply in the

https://doi.org/10.1346/CCMN.2001.0490607 Published online by Cambridge University Press

Table 3. Representative microprobe analyses (wt.%) and structural formulae[1] of chamosite from the Kremikovtsi SIF.

Mode of occurrence	Replacement		Vug filling			Vug lining					Fracture filling				
Polytype	*Ib*(β = 90°)		*Ib*(β = 90°)			*Ib*(β = 90°)					*IIb*(β = 97°)				
Sample #	K-1023/1		K-1023/2			K-1032					K-1A		K-1B		
SiO_2	24.23	24.99	25.27	25.89	25.94	23.97	25.70	24.40	25.84	24.90	20.79	25.58	22.85	23.54	23.70
Al_2O_3	23.50	23.43	24.52	24.80	24.91	22.48	23.27	22.64	23.69	22.85	18.17	21.73	18.74	19.12	18.99
Fe_2O_3	3.74	3.96	3.85	3.94	3.87	3.64	3.41	3.58	3.59	3.60	3.47	4.25	3.99	3.63	3.71
FeO	30.28	32.08	31.19	31.88	31.35	29.49	27.59	28.95	29.06	29.19	28.13	34.39	32.31	29.39	30.08
MnO	0.31	0.15	0.20	0.32	0.31	0.30	0.45	0.31	0.61	0.32	1.83	0.70	0.64	0.22	0.31
MgO	5.36	4.51	5.47	5.27	5.80	5.31	5.90	5.28	6.06	5.77	2.54	6.04	4.97	5.91	6.57
Na_2O	0.19	0.10	0.28	0.22	0.43	0.12	0.64	0.15	0.59	0.10	n.d.	n.d.	n.d.	n.d.	n.d.
K_2O	n.d.[2]	n.d.	n.d.	n.d.	n.d.	n.d.	0.28	n.d.	0.10	n.d.	n.d.	n.d.	n.d.	n.d.	n.d.
Total	87.61	89.22	90.78	92.32	92.61	85.31	87.24	85.31	89.54	86.73	74.93	92.69	83.50	81.81	83.36
Si	2.650	2.699	2.662	2.684	2.674	2.690	2.780	2.725	2.738	2.731	2.734	2.698	2.704	2.780	2.757
^{IV}Al	1.350	1.301	1.338	1.316	1.326	1.310	1.220	1.275	1.262	1.269	1.266	1.302	1.296	1.220	1.243
^{VI}Al	1.680	1.681	1.706	1.713	1.700	1.664	1.746	1.705	1.697	1.685	1.550	1.399	1.318	1.441	1.360
Fe^{3+}	0.308	0.322	0.305	0.308	0.300	0.308	0.278	0.301	0.287	0.297	0.343	0.337	0.356	0.322	0.324
Fe^{2+}	2.770	2.897	2.748	2.763	2.702	2.768	2.496	2.704	2.576	2.677	3.093	3.034	3.197	2.903	2.926
Mn	0.029	0.014	0.018	0.028	0.027	0.028	0.041	0.030	0.055	0.030	0.204	0.063	0.064	0.022	0.031
Mg	0.874	0.726	0.859	0.814	0.891	0.888	0.951	0.879	0.957	0.943	0.498	0.949	0.877	1.040	1.139
Σ Oct	5.661	5.640	5.636	5.626	5.620	5.656	5.512	5.619	5.572	5.632	5.688	5.782	5.812	5.728	5.780
Na	0.041	0.021	0.057	0.044	0.085	0.026	0.134	0.032	0.121	0.021	n.d.	n.d.	n.d.	n.d.	n.d.
K	n.d.	n.d.	n.d.	n.d.	n.d.	n.d.	0.039	n.d.	0.014	n.d.	n.d.	n.d.	n.d.	n.d.	n.d.
Fe/(Fe + Mg)	0.779	0.816	0.780	0.790	0.771	0.776	0.745	0.774	0.749	0.759	0.873	0.780	0.802	0.756	0.740
Mg/Fe	0.284	0.226	0.281	0.265	0.297	0.289	0.343	0.293	0.334	0.317	0.145	0.282	0.247	0.322	0.350
Al/Si	1.143	1.105	1.144	1.129	1.132	1.106	1.067	1.094	1.081	1.082	1.030	1.001	0.967	0.957	0.944
Al/(Al + Si)	0.533	0.525	0.533	0.530	0.531	0.525	0.516	0.522	0.519	0.520	0.507	0.500	0.492	0.489	0.486
Fe/(Al + Si + Fe)	0.351	0.362	0.349	0.350	0.345	0.352	0.326	0.345	0.334	0.343	0.382	0.384	0.401	0.372	0.377

[1] Formulae calculated assuming 10% Fe = Fe^{3+}, Σ + charges = 28.00.
[2] n.d. — not detected.

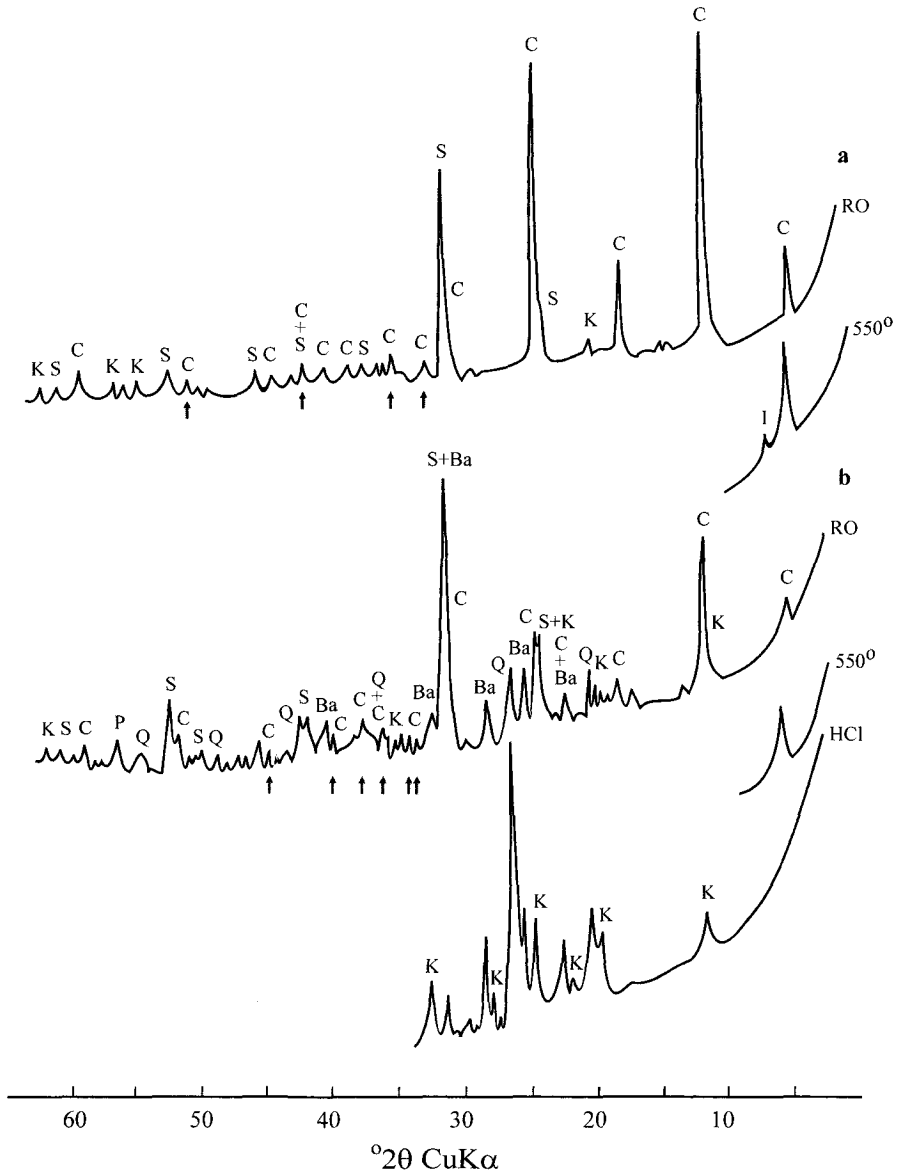

Figure 7. XRD patterns of air-dried randomly oriented (RO) chamosite-dominated aggregate samples, heated at 550°C, and treated with hot HCl, from the Kremikovtsi SIF. (a) Vug-lining rosette chamosite of the *Ib*(β = 90°) group. (b) Fracture-filling chamosite of the *IIb* group. Ba—barite; C—chamosite; K—kaolinite; P—pyrite; Q—quartz; S—siderite; (+)—peak coincidence. Diagnostic reflections of chlorite groups are also marked.

Middle Triassic sedimentary basin was extremely low, represented only by single micaceous flakes and K-feldspar grains, and rare fossil remains (Damyanov, 1996, 1998).

The main illitic material ('sericite' is the widely adopted petrographic term in this case) in the Kremikovtsi SIF belongs to the barite-sulfide assemblage. Vug-filling I-S forms aggregates, up to 10 μm in diameter, of stick plates with scalloped and slightly curled edges (Figure 8b). Parallel aggregates of irregular platy crystallites which are twice as large, with elongated spines and scalloped pointed edges, supplemented with I-S 'ribbons', form linings on the walls of small solution vugs (Figure 8c). Study by TEM showed that both vug-lining and vug-filling I-S consisted mainly of well defined elongated platy particles (Figure 8d). Such a habit is characteristic of authigenic I-S crystallized directly from solution in open space (Yau *et al.*, 1988), but not of conventional detrital clay sediments in which pseudoisometric particles are predominant (Kotelnikov and Konyukhov, 1986).

Aggregates of recrystallized subequant plates with stubby spines and distinct preferred orientation, associated with granoblastic quartz, form fracture fillings

https://doi.org/10.1346/CCMN.2001.0490607 Published online by Cambridge University Press

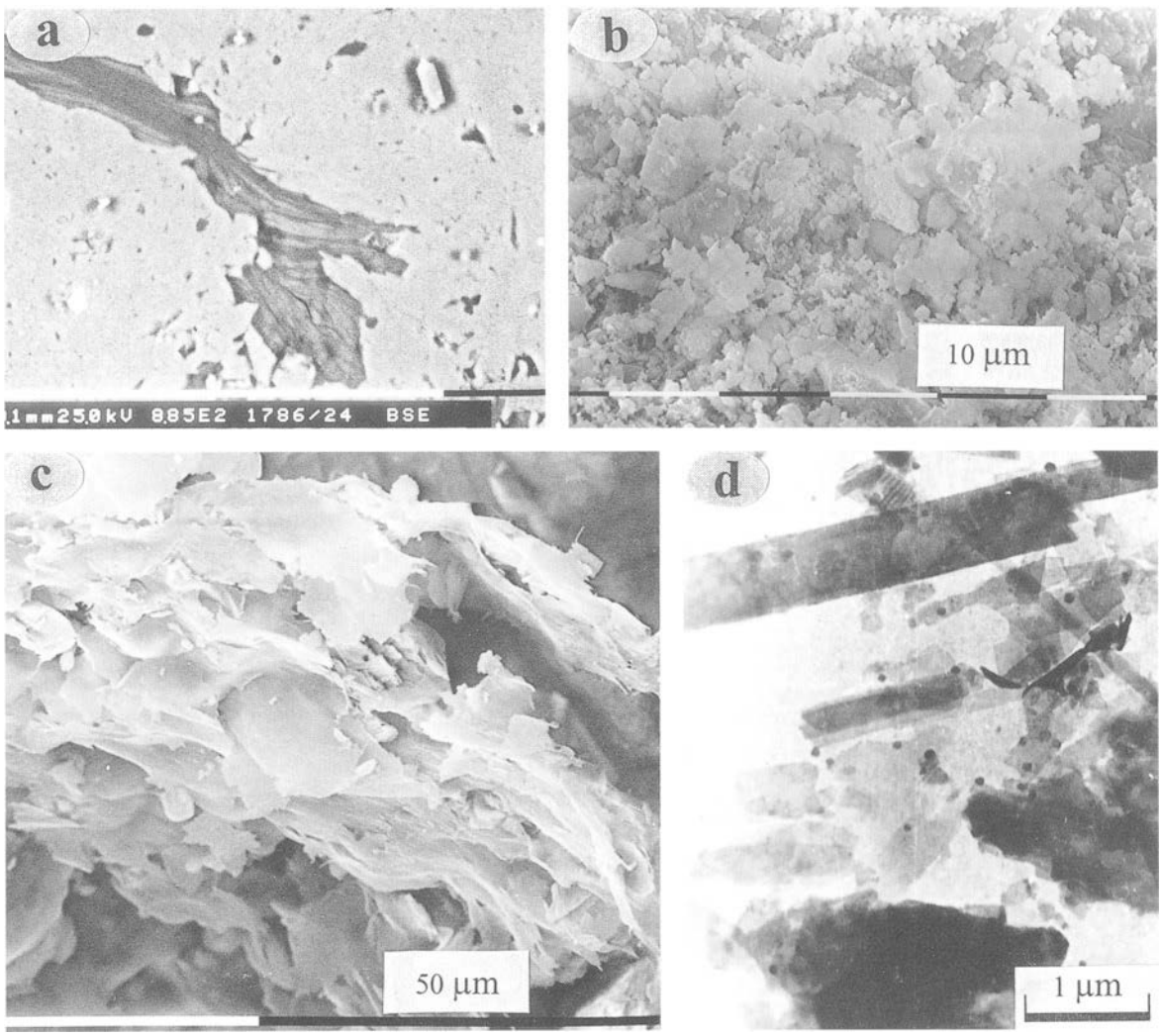

Figure 8. Photomicrographs of I-S from the Kremikovtsi SIF. (a) BSE image of a fine-scale incoherent intergrowth between illite (dark strands) and chamosite (light strands) in a detrital flake of degraded low-grade metamorphic mica; sparry siderite matrix (gray). (b) Stick plates of vug-filling I-(8–11%)S scalloped and slightly curled at the edges; SE image. (c) Parallel aggregates of irregular elongated flat crystallites of vug-lining I-(6–8%)S. Note the scalloped pointed edges of platy particles, supplemented with I-S 'ribbons'. SE image; (d) TEM image of elongated platy particles of vug lining I-(6–8%)S.

in a matrix of bulk granoblastic siderite in local zones of tectonically induced low-grade dynamic metamorphism.

The XRD patterns of authigenic I-S (Figure 11a, b) give the following basic information, based on the criteria summarized by Środoń and Eberl (1984): (1) it is a mixed-layer phase because the presence of a series of basal reflections of varying width; (2) it has an expanding component (Ir $>$ 1 and change of peak positions and intensities after glycolation); (3) the expandability is slightly greater in the vug-lining variety in a common interval of 6–11%; (4) type of ordering is R $\geq$ 3; (5) one water-layer complex is present as the 5 Å reflection of solvated preparations is broad, weak and displaced toward smaller 2θ angles and the 3.33 Å reflection is sharp, strong and slightly displaced toward larger angles (Horton, 1983); (6) the 1.499 Å d_{006} value indicates low (Fe + Mg) contents in the octahedral positions, as shown in Table 4.

We found no I-S with expandability $>$12% during our investigations. As Andreeva *et al.* (1989) concluded on the basis of XRD and TEM studies of more than 500 samples, the absence of mixed-layer I-S with high ($>$50%) expandability (excluding some Na and Ca varieties examined by Inoue and Utada, 1983) and ordered interlayering (or tendency toward ordering) are important features of hydrothermal mineral formation, unlike the sedimentary-epigenetic sequences in which there exists a full range of expandability.

https://doi.org/10.1346/CCMN.2001.0490607 Published online by Cambridge University Press

Table 4. Microprobe analyses[1] (wt.%) and structural formulae[2] of detrital mica and I-S from the Kremikovtsi SIF.

Mode of occurrence	Detrital	Vug filling	Vug lining	Fracture filling
% of smectite	<5	8–11	6–8	<5
Polytype	$2M_1$ (?)	$1M$	$1M \gg 2M_1$	$2M_1 \gg 1M$
Sample #	K-1034	K-1023/1	K-1032/1	K-2
SiO_2	46.04	48.62	48.89	49.03
Al_2O_3	31.62	32.95	33.37	31.75
TiO_2	0.35	n.d.[3]	n.d.	0.20
Fe_2O_3	2.01	1.54	0.40	1.68
FeO	0.45	0.35	0.09	0.38
MnO	0.12	n.d.	n.d.	n.d.
MgO	1.45	1.56	0.76	1.46
CaO	n.d.	n.d.	n.d.	0.03
Na_2O	0.94	0.08	0.60	0.01
K_2O	9.10	7.73	7.28	9.36
Total	92.08	92.83	91.39	93.90
Si	3.162	3.244	3.286	3.271
^{IV}Al	0.838	0.756	0.714	0.729
^{VI}Al	1.722	1.836	1.930	1.768
Ti	0.018	n.d.	n.d.	0.010
Fe^{3+}	0.104	0.077	0.020	0.084
Fe^{2+}	0.026	0.020	0.005	0.021
Mn	0.007	n.d.	n.d.	n.d.
Mg	0.149	0.155	0.076	0.145
Σ Oct	2.026	2.088	2.031	2.028
Ca	n.d.	n.d.	n.d.	0.002
Na	0.125	0.010	0.078	0.002
K	0.797	0.658	0.624	0.797
Σ Int	0.922	0.668	0.702	0.801
Al/Si	0.810	0.799	0.805	0.763
$Fe^{3+}/(Fe^{3+} + {}^{VI}Al)$	0.055	0.040	0.010	0.045

[1] Average of five analyses for a sample.
[2] Formulae calculated assuming an Fe^{2+}/Fe^{3+} ratio of 1:4 and Σ + charge = 22.00.
[3] n.d. = not detected.

The XRD studies of randomly oriented authigenic I-S aggregate samples show that $1M$ is the dominant polytype either as a sole polytype variety (Figure 11c, d) or in a mixture with small amounts (traces) of $2M_1$. As a rule, I-S polytype homogeneity was considered to be evidence of a one-stage process of mineral formation (Drits and Kossowskaya, 1991) and characteristic of low-temperature (*i.e.* ≤250°C) I-S from zones of hydrothermal alteration of ore deposits (Omelyanenko *et al.*, 1982; Rusinova and Rusinov, 1986; Eberl *et al.*, 1987; Andreeva *et al.*, 1989) as well as for ore deposits formed at a small depth under the surface (Rusinova and Rusinov, 1986).

Vug-filling I-S has a slightly higher expandability than vug-lining I-S (Figure 11a, b). Both types of authigenic I-S have almost perfect $1M$ structures, as shown by the sharpness of the peaks and by the absence of the 22–33°2θ band indicating structural defects (mainly $\pm n60°$ rotational stacking faults, Drits *et al.*, 1984) (Figure 11c, d). The lack of 111 reflections at 3.87 Å and the appearance of shoulders toward larger 2θ angles at 2.40 Å peaks specify *T*-stacking of layers (*trans* positions vacant in the octahedral sheet).

Fracture-filling I-S from tectonically reworked zones is $2M_1$-polytype dominated (Figure 11e), thus indicating higher P-T conditions (≥280°C) of low-grade dynamic metamorphism. No $1M_d$ polytype varieties, typical of diagenetic sedimentary sequences and initial stages of anchizone, were found in the Kremikovtsi SIF. That appears to be a characteristic feature of hydrothermal I-S, as noted by Andreeva *et al.* (1989).

The microprobe study showed a good compositional homogeneity for each type of I-S with a standard deviation too statistically insignificant to be noted (Table 4). Such an homogeneity, coupled with a relatively uniform size and shape, was reported by Yau *et al.* (1988) as implying direct crystallization from solution in a single, short-lived, episodic hydrothermal event.

Authigenic illitic material is chemically I-S in which pyrophyllite substitutions are present (the layer charges originate principally through substitution of Al for Si in tetrahedral sites) (Figure 9a). The vug-lining variety is more aluminous and siliceous, and with a greater degree of interlayer occupancy and a larger Na content (~11% of paragonitic component), unlike the vug-filling I-S which is 2.5 times more abundant in (Fe + Mg) (Table 4; Figures 9, 10). Interlayer cation deficiency ranging from 0.30–0.33 is compensated structurally by an increase in Si in the tetrahedral sites and in bivalent cations at the expense of Al in the octahedral positions. Thus, besides the aforementioned

morphological and structural differences, authigenic I-S differs chemically in conformity with its mode of occurrence (formation).

As can be seen in Figure 9b–d, our data are consistent with the relations 'composition-type of polytype' and "composition-expandability", suggested by Andreeva *et al.* (1989), falling entirely within the delineated fields. These authors noticed that the discrimination fields have areas of overlap and thus, of uncertainty, yet some general tendencies are significant. Summarizing a large volume of data, they found several relatively well-defined compositional constraints to distinguish hydrothermal from sedimentary-epigenetic (but not late epigenetic, which is compositionally close to hydrothermal) I-S, namely: (1) greater total Al (generally $\Sigma Al > 2$; $2.5 < \Sigma Al < 3$, for 'sericite') (Figure 9e); (2) smaller Si contents ($0.5 < {}^{IV}Al < 1.0$) (Figure 9e, f); (3) fewer bivalent cations in the octahedral sites (typically up to 20% from the total octahedral occupancy) (Figure 10b).

Drits and Kossowskaya (1991) proposed another criterion, considered to be an important feature of illitic material, to delineate between the dioctahedral micaceous minerals, the $Fe^{3+}/(Fe^{3+} + {}^{VI}Al)$ ratio, which is up to 0.05 for hydrothermal I-S (Figure 10c). Plotting our data onto the diagrams mentioned above, their unambiguous affiliation to the fields of hydrothermal I-S can be seen.

The compositional comparison between the illitic material from the Kremikovtsi SIF and illites in iron formations and ironstones shows good agreement only for the fracture-filling variety (Figure 10a). This is understandable because most of the sedimentary iron ores underwent intensive pre-metamorphic alterations comparable with the dynamometamorphic alterations in the Kremikovtsi SIF. It is also noteworthy that the compositions of I-S studied, even though associated in places with chamosite (Figure 5c), are not relevant to the typical equilibrium illite-chlorite assemblage in dia-epigenetic sequences (point D in Figure 10a), thus implying subsequent crystallization under different formation conditions (probably at a gradual increase in pH; see Figure 13c).

Recrystallized fracture-filling I-S differs from the authigenic varieties in both pyrophyllitic and celadonitic substitutions, greater interlayer occupancy ($\Sigma Int = 0.80$), and lower total Al and ${}^{VI}Al$ contents.

Kaolinite

Authigenic kaolinite associated with barite, sulfides and other phyllosilicates (radial bladed berthierine, chamosite, I-S) was observed macroscopically as small white nests, veinlets or partings in the otherwise gray siderite host. Generally, it is represented by stacked aggregates of randomly oriented platelets (Figure 12a). Slightly elongated pseudohexagonal plates and booklets (Figure 12b) as well as vermicular-type stackings (Figure 12c) were also observed occasionally. The close association with berthierine barite, and the sulfides notwithstanding, the kaolinite crystals formed intergrowths with these minerals only along the outer parts of their own aggregates, not within them. This structural relationship implies intensive initial crystallization of kaolinite followed by a transition period of common growth by formation of barite/sulfides.

The XRD patterns of kaolinite indicated a high degree of 'crystallinity' (Hinckley index varies between 1.30 and 1.40). The microprobe study gave no significant compositional differences in comparison with the standard data, with negligible traces of Fe, Mg, Mn and K near the detection limits of the microprobe.

Thus, this low-defect kaolinite with typical authigenic morphology and practically stoichiometric standard composition indicates crystallization from solution in open spaces accompanying (but anticipating) the barite-sulfide deposition. Keller (1988) considered kaolinite with similar characteristics, coexisting with sulfide minerals, to be an important mineralogical indicator of a regional thermal event causing the formation of the Mississippi Valley type Zn-Pb ore deposits in the mid-continent United States.

DISCUSSION

Phyllosilicates in the general sequence of mineral formation in the Kremikovtsi SIF

Two main episodes of layer-silicate authigenesis can be distinguished in the Kremikovtsi SIF: (1) an advanced stage of early diagenesis; and (2) superimposed epigenetic hydrothermal deposition in open spaces (Figure 13).

As is known (Curtis and Spears, 1968; Eugster and Chou, 1973; Maynard, 1983), siderite precipitation takes place under conditions of low sulfide-ion concentration, high carbonate-ion accumulation and high Fe^{2+}/Ca ratio, low Eh, and pH close to 7. The hydrothermal sedimentation of siderite at Kremikovtsi was accompanied by extremely low detrital input (not only *in situ*, but also in the whole sedimentary basin) which indicates the leading role of chemical processes in mineral formation. Thus, most mineral-forming elements (Fe, Mn, Si, Al, C, partially Mg, *etc.*) in the SIF derived from an external source—hydrothermal solution venting onto the sea bottom, as was indicated in a previous paper (Damyanov, 1998).

Early diagenesis started with microsparitization of initial femicrite followed by neomorphic overgrowths of sparry siderite rims attached to the microsparite nuclei. These outer zones of sparry siderite grains are richer in Mg than the inner ones (Damyanov, 1998) reflecting the increase of Mg activity at the expense of Fe and Mn in solution. The process of sparitization exhausted the CO_2 concentration in pore-water, leading

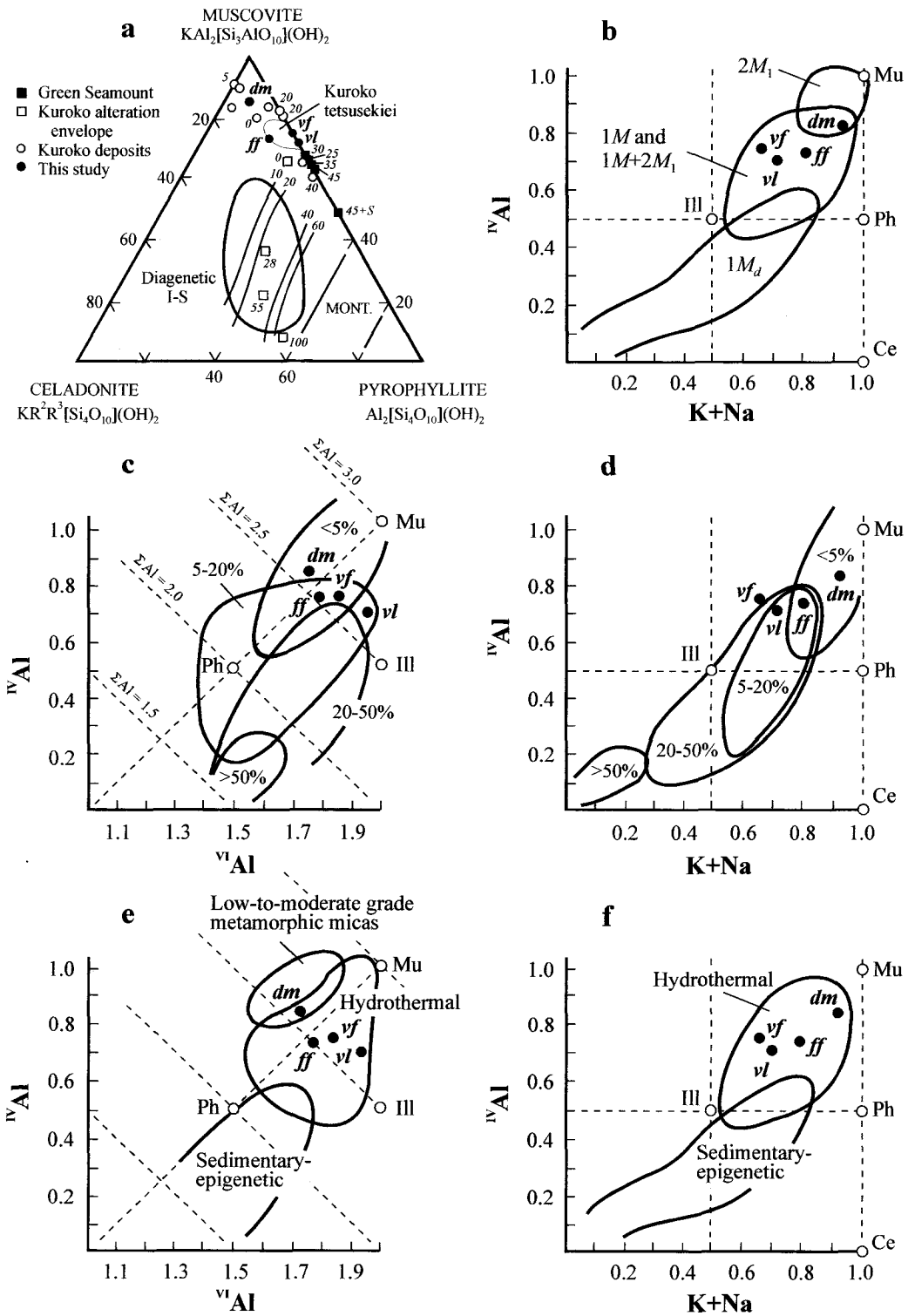

Figure 9. Chemical compositions (molar basis) of detrital mica (*dm*), vug-filling (*vf*), vug-lining (*vl*), and fracture-filling (*ff*) I-S from the Kremikovtsi SIF plotted on: (a) a ternary muscovite-celadonite-pyrophyllite diagram (after Hower and Mowatt, 1966). Data for I-S from the Kuroko massive sulfide deposits (Sudo and Shimoda, 1978), the hydrothermally altered rocks around the Kuroko deposits (Inoue and Utada, 1983), the Kuroko tetsusekiei (tuffaceous exhalite overlying sulfide deposits; Kalgeropoulos and Scott, 1985), and from recent massive sulfide deposits at Green Seamount near the East Pacific Rise (Alt and Jiang, 1991) are also shown. (b-f) Binary ^{IV}Al *vs.* ^{VI}Al and ^{IV}Al *vs.* K+Na diagrams showing the relationships between

https://doi.org/10.1346/CCMN.2001.0490607 Published online by Cambridge University Press

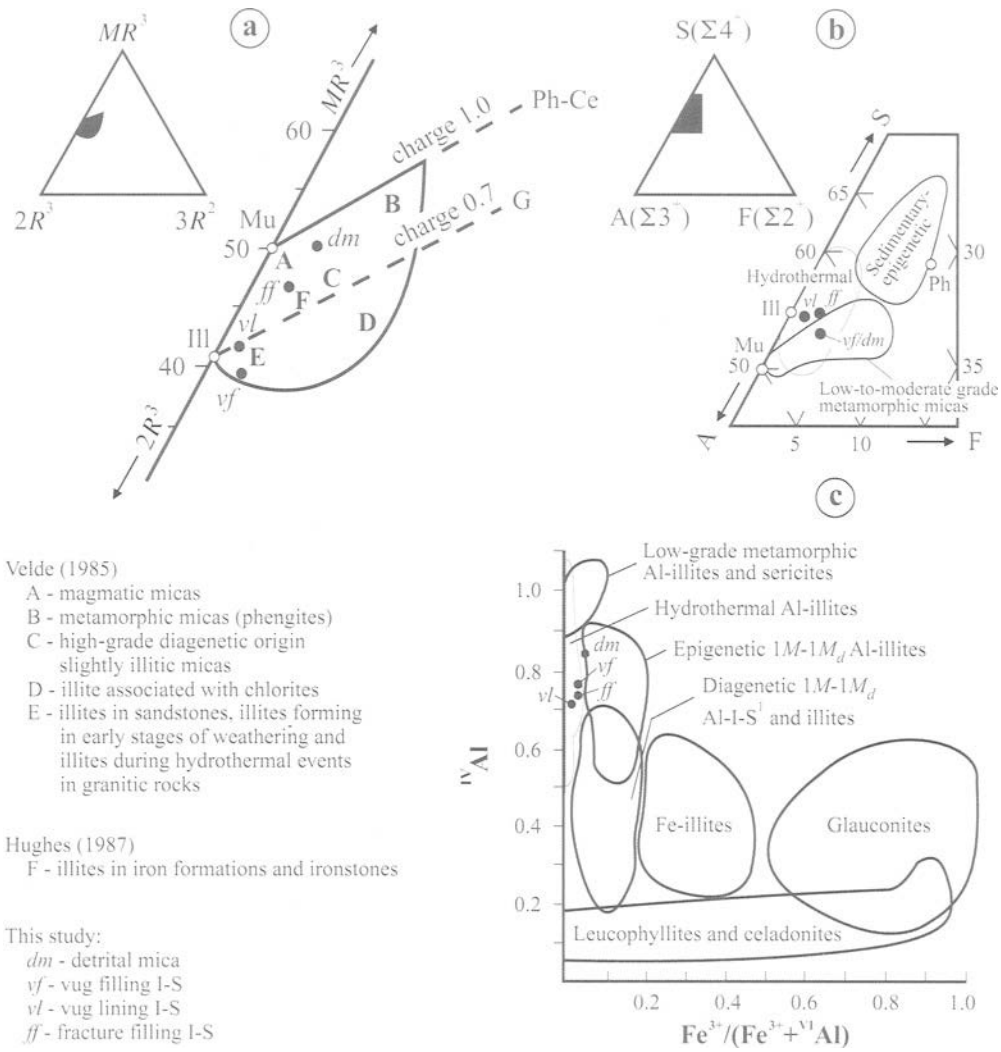

Figure 10. Chemical compositions (molar basis) of I-S from the Kremikovtsi SIF plotted on: (a) an MR^3-$2R^3$-$3R^2$ diagram of illite compositions near the muscovite corner (after Velde, 1985); (b) simplified $\Sigma 2^+$-$\Sigma 3^+$-$\Sigma 4^+$ diagram of I-S (after Andreeva *et al.*, 1989); (c) ^{IV}Al *vs.* $Fe^{3+}/(Fe^{3+}+{}^{VI}Al)$ diagnostic diagram of dioctahedral micaceous minerals (after Drits and Kossovskaya, 1991). [1] The original term used by the authors is hydromica. Character symbols as in Figure 9. G—glauconite-type composition; Ph-Ce—phengite-celadonite compositions.

to increase in silica activity and intensive chert precipitation as an intergranular cement, catalyzed by the high Mg content (Kastner, 1979) and increased alkalinity provided for the carbonate surroundings. As noted by Harder (1978), low silica concentration in solution is the most important condition for low-temperature synthesis of iron clay minerals (see also Figure 14). The other favorable factors (high Mg content, high pH and strongly reducing conditions), characteristic of marine carbonate diagenesis, were also available, in addition to the Fe content which was still high enough to have been incorporated into a layer silicate structure. Thus, berthierine formation should be addressed to the advanced stage of early diagenesis when silica concentration was low enough to allow iron silicate crystallization.

The high Mg activity in pore-water caused the formation of berthierine rich in Mg. This is characteristic

←

the compositional variations and the polytypes (b), % expandable layers (c, d), and genetic affiliations (e, f) of I-S (after Andreeva *et al.*, 1989, based on their own works and the results from >130 other works, simplified). Theoretical end-member compositions: Ce—celadonite; I—illite; Mu—muscovite; Ph—phengite.

https://doi.org/10.1346/CCMN.2001.0490607 Published online by Cambridge University Press

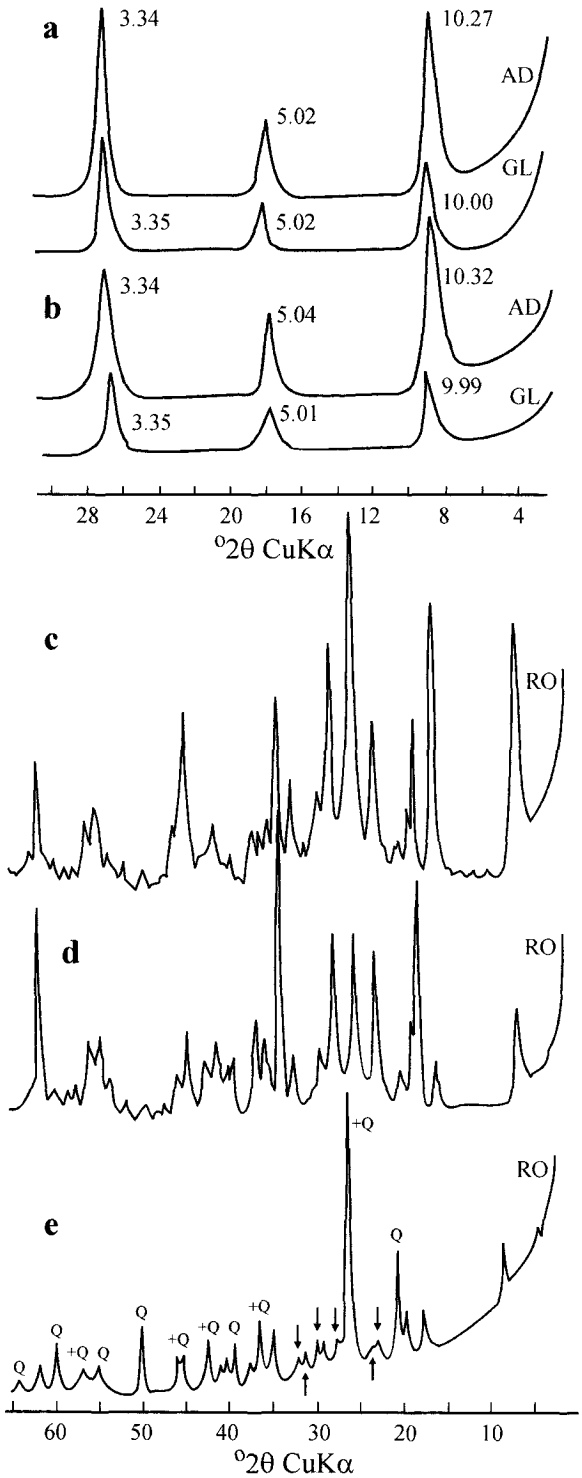

Figure 11. Representative XRD patterns of air-dried oriented (AD), glycolated (GL), and randomly oriented (RO) aggregate samples of vug-lining (a, d), vug-filling (b, c), and fracture-filling (e) I-S from the Kremikovtsi SIF. (a) I-(6–8%)S, Ir = 1.26, Kübler index = 7.5; (b) I-(8–11%)S, Ir = 1.40, Kübler index = 8.5; (c, d) 1*M* I-S; (e) $2M_1$ I-S. Q—quartz; (+)—peak coincidence. Diagnostic reflections of $2M_1$polytype are also marked (e).

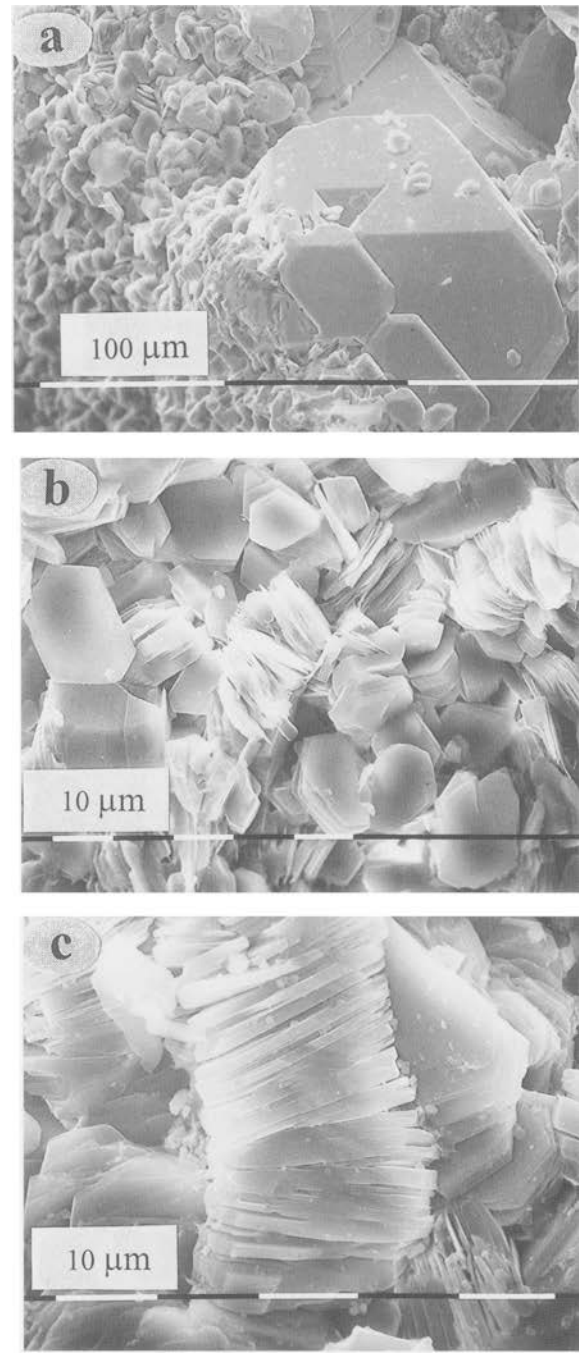

Figure 12. SE photomicrographs of kaolinite from the Kremikovtsi SIF. (a) Stacks of randomly arranged kaolinite platelets associated with euhedral barite crystals. Note that the growth of kaolinite plates on the barite faces started before the barite crystal growth ended, thus implying a process of common growth, as shown for the barite-chamosite intergrowths in Figure 6c. (b) Slightly elongated plates and booklets of kaolinite. (c) Vermicular-type stacking of kaolinite.

https://doi.org/10.1346/CCMN.2001.0490607 Published online by Cambridge University Press

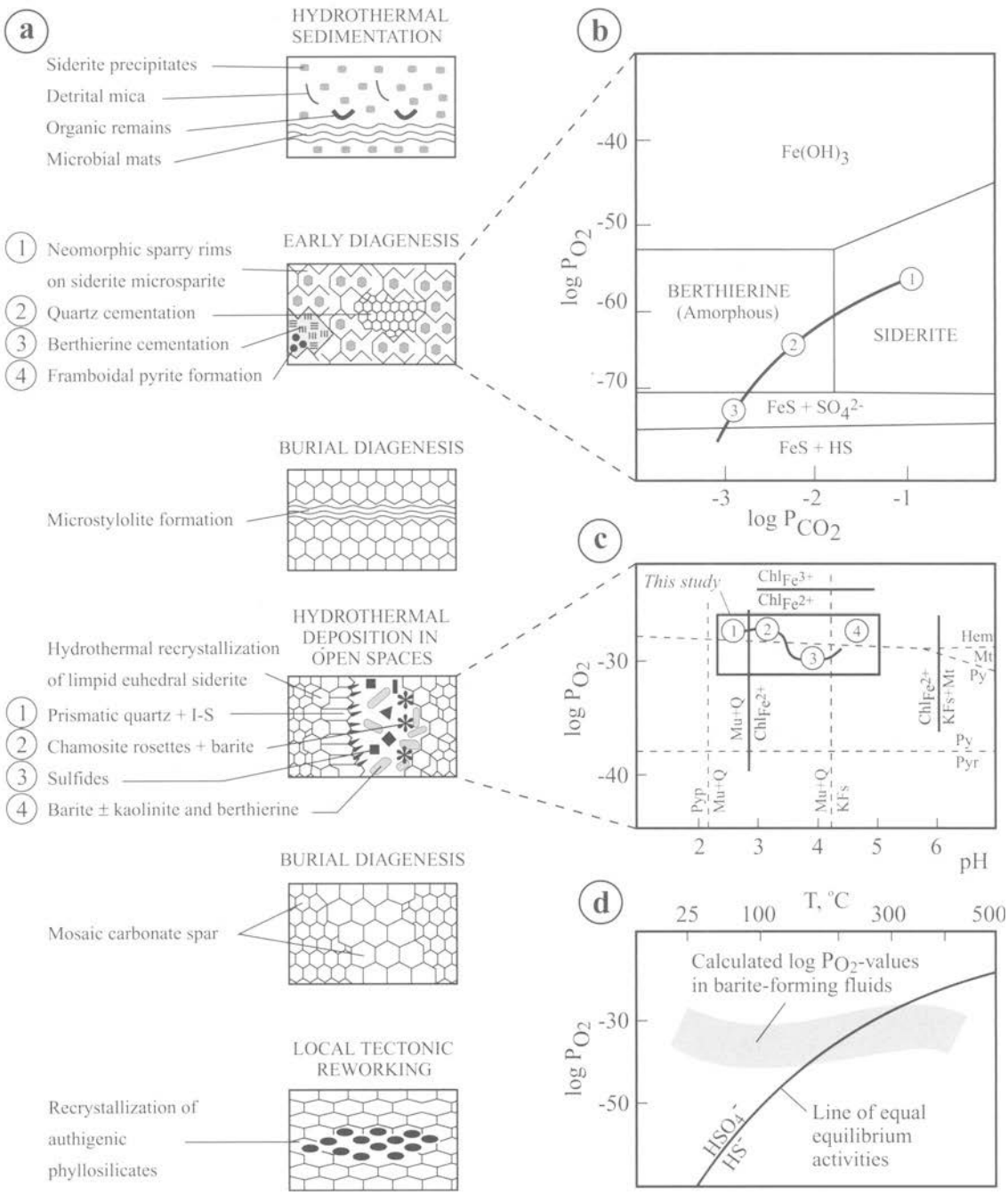

Figure 13. Generalized sketch of proposed phyllosilicate mineral formation in the Kremikovtsi SIF. (a) Schematic sequence of ore formation based on the petrographic features observed. The whole petrographic variety of carbonate diagenesis (*e.g.* insignificant intraclastic resedimentation, microsparitization of initial micrite, *etc.*) and hydrothermal deposition in open spaces is not included. Not to scale. (b) Stability relations among siderite-berthierine-FeS-Fe(OH)$_3$ as a function of P_{CO_2} and P_{O_2} at pH = 8, S = 10^{-6} (Maynard, 1983). The hypothetical generalized trends of proposed development of mineral formation are presented by arrows. (c) Phase equilibrium and stability fields of hydrothermal mineral formation at 200–300°C, [K^+] = 0.1 mol/L, and [ΣS] = 0.01 mol/L as a function of pH and P_{O_2} (after Rusinova *et al.*, 1986). The shaded area limits the field of ferrous chlorites. Chl^{2+}—ferrous chlorite; Chl^{3+}—ferric chlorite; Hem—hematite; KFs—K-feldspar; Mt—magnetite; Mu—muscovite; Py—pyrite; Pyr—pyrrhotite; Pyp—pyrophillite; Q—quartz; (d) log P_{O_2} as a function of temperature of hydrothermal barite formation (after Tvaltschrelidze and Scheglov, 1990).

https://doi.org/10.1346/CCMN.2001.0490607 Published online by Cambridge University Press

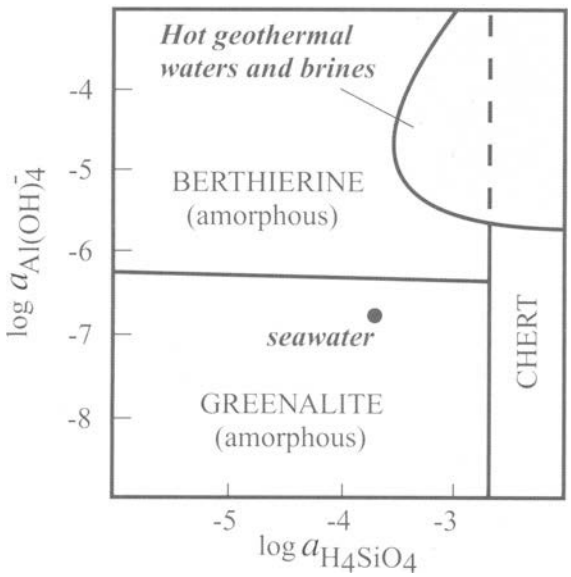

Figure 14. Stability fields of berthierine, greenalite and chert as a function of activities of Si and Al complexes in water systems. After Maynard (1983), with additional data (18 analyses) for mainly metalliferous hot geothermal waters and brines, compiled from Ellis (1967), White (1967), Dickson and Tunell (1968), Emery *et al.* (1969), Weissberg *et al.* (1979).

of authigenic crystallization from Mg-enriched pore-waters (*i.e.* marine diagenetic or non-marine with high seawater input) (Figure 15). In contrast, the other type of Mg-rich berthierine is from zones of pre-ore metasomatism where destructured femic minerals are the main source of Mg. Berthierine formation caused a decrease in O_2 in this closed pore-water system of advanced diagenesis and initiated bacterial reduction of seawater sulfate to form framboidal pyrite (initial Fe monosulfide).

Burial diagenesis started with microstylolite formation and gradual recrystallization of the carbonate matrix. The temperature of complete transformation of berthierine into more stable chamosite is a debatable question, but according to Iijima and Matsumoto (1982) it ranges from 130 to 160°C. Because a similar T_{max} of burial diagenesis is proposed for the Kremikovtsi SIF, most of the berthierine transformed into chamosite.

Epigenetic hydrothermal activity probably attacked the siderite sediment at the stage of advanced lithification. The invasion of hot, strongly aggressive, acid hydrothermal solution into a carbonate medium provoked intensive dissolution controlled by the initial microtectonic framework.

As mentioned above, $^{VI}Al > {}^{IV}Al$ in hydrothermal chamosite implies an acid environment of formation because the total quantity of bivalent cations (stronger alkalis) in the octahedral sites decreases at almost con-

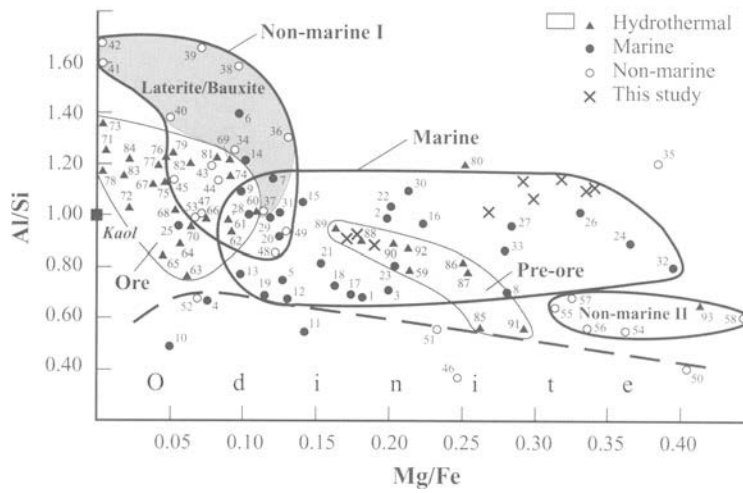

Figure 15. Mg/Fe *vs.* Al/Si plot of compositional variations of berthierines formed in different geological settings. Marine: ironstones — 1 (MacGregor *et al.*, 1920), 2 (Hallimond, 1939), 3 (Engelhardt, 1942), 4–5 (Deverin, 1945), 6 (Brindley, 1951), 7 (Brindley and Youell, 1953), 8 (Deudon, 1955), 9 (Protich, 1955), 10–14 (Bubenicek, 1961), 15 (Halbach, 1970), 16 (Shilin *et al.*, 1979), 17–27 (Maynard, 1986), 28–31 (Lu *et al.*, 1994); iron formations — 32 (Floran and Papike, 1975); marine breccia — 33 (Velde *et al.*, 1974). Non-marine: laterite/bauxite — 34 (Brindley, 1951), 35–37 (Yershova *et al.*, 1976), 38–40 (Klekl, 1979), 41–42 (Toth and Fritz, 1997); coal measures — 43–45 (Iijima and Matsumoto, 1982); brackish water — 46 (Rohrlich *et al.*, 1969), 47 (Thurrell *et al.*, 1970), 48–49 (Taylor, 1990); modern delta — 50–51 (Porrenga, 1966), 52 (Rude and Aller, 1989); modern desert soil — 53 (Kodama and Foscolos, 1981); deltaic/estuarine complex — 54–58 (Hornibrook and Longstaffe, 1996). Hydrothermal: ore — 59 (Sudo, 1943), 60–75 (Rusinova *et al.*, 1986), 76–80 (Slack *et al.*, 1992), 81–84 (Jiang *et al.*, 1992); pre-ore — 85 (Novak *et al.*, 1959), 86–92 (Rusinova *et al.*, 1986); ultramafic dyke serpentinization — 93 (Arima *et al.*, 1985).

https://doi.org/10.1346/CCMN.2001.0490607 Published online by Cambridge University Press

stant Si/Al ratios in the tetrahedral positions (Rusinova *et al.*, 1986). The excess of octahedral charge is compensated by a decrease of total octahedral cations. The second important factor in the system, the P_{O_2}, may have relatively low values, shown as much by the absence of iron oxide minerals as by the strong domination of ferrous chamosite.

A proposed sequence of mineral formation in the barite-sulfide assemblage associated with the phyllosilicates described, is presented in Figure 13c on the basis of petrographic observations. This generalized sequence may be expressed, with many reservations, as follows: (1) prismatic quartz-I-S; (2) chamosite rosettes-barite; (3) barite-sulfides-bladed chamosite; (4) kaolinite-berthierine-barite. The common trend is controlled by the gradual alkalinity of solution at a slightly varied P_{O_2} near the sulfide/sulfate stability boundary.

Barite plays a key role in understanding such a paragenetic association (barite-sulfides-phyllosilicates) where there is no indication of repeated input of late hydrothermal fluids (no mutual corrosion faces). As can be seen in Figure 13d, at the temperature of barite formation in the Kremikovtsi SIF (200–230°C) and $P_{O_2} \approx -30$, the barite-forming fluids may consist of two antipathetic soluble complexes of S in a metastable equilibrium and therefore allow the space- and time-bound (in a geological sense) crystallization of layer silicate, sulfate and sulfide phases. Thus, the hydrothermal-epigenetic layer silicates probably formed from an acidic (pH = 3–5), hot (200–250°C), hydrothermal solution under relatively stable reducing conditions (log P_{O_2} slightly lower than −30, *i.e.* near the sulfide/sulfate stability boundary) (Figure 13c, d).

What is the reason for the formation of structurally (and thermodynamically?) metastable berthierine *vs.* stable chamosite as an authigenic (not controlled by an initial precursor) phase under hydrothermal conditions? Rusinova *et al.* (1986) proposed an explanation related to mode of formation and crystallization kinetics. According to those authors, the most favorable conditions of metastable mineral formation in hydrothermal processes existed during (or shortly after) the invasion of solution into open spaces, at a sudden drop in temperature, or abrupt changes of acidity. Such an explanation is applicable to the hydrothermal berthierine from the Kremikovtsi SIF, which was found as vug fillings conserved after the monostage hydrothermal activity, thus preventing replacement by chamosite from a new portion of fluids. The temperature factor controlling berthierine stability under burial diagenetic conditions thereafter should be excluded because of the higher temperature of its initial formation.

In addition to the two main episodes of phyllosilicate authigenesis described above, aggregates of layer silicates recrystallized locally in tectonically deformed zones of lowest-grade anchimetamorphism.

Controls on phyllosilicate mineralogy in carbonate-hosted SEDEX SIFs: hydrothermal-sedimentary vs. hydrothermal-epigenetic mineral formation

As noted by Maynard (1983), the obvious differences in phyllosilicate mineralogy of iron formations and ironstones were controlled by the initial Al concentrations at the sites of mineral formation. Seawater enriched in Fe mainly from hydrothermal exhalations in deep basinal zones moved to shallow-water shelf areas where cherty iron formations in distinct facies precipitated. The separation of Al from Fe may have been realized before the start of the movements of deep water by the upwelling because of the very low migration ability of Al which is characterized by an extremely low coefficient of water migration, ~0.01 (Perelman, 1989). Thus, the low Al concentration in seawater predetermines the formation of low to non aluminous phyllosilicates (greenalite, stilpnomelane) during diagenesis of iron formations (Figure 14).

Higher Al contents in the mineral-forming water are needed to form aluminous layer silicates, such as berthierine, glauconite and illite. This condition is available in coastal areas where intensive weathering provides for a large quantity of terrigenous material including kaolinite and/or smectite particles. It seems likely for these particles to have served as initial precursors of diagenetic Fe-Al phyllosilicates which are a major constituent of ironstones (Bhattacharyya, 1983).

In the SEDEX iron formations, which developed in a geological setting of arid climate, low terrigenous input, and weak transportation ability, the main source of metals is hydrothermal solution mixed with seawater in variable proportions. Practically all recent hot geothermal waters and brines contain Al concentrations much greater than those in seawater (Figure 14), thus indicating the dominant role of aluminous phyllosilicates (in particular of berthierine) in the SEDEX SIFs. This conclusion should not be changed even if the layer silicate formation took place not only by precipitation from solution, but also by progressive transformation of initial precursor (kaolinite, illite) or by replacement of volcaniclastic materials.

Thus, based on the analysis of petrographic observations and their good coherency to thermodynamic constraints (Figure 13), the phyllosilicate mineralogy of hydrothermal-sedimentary facies of carbonate-hosted cherty SIFs should be considered to be a result of precipitation during progressive diagenesis under anoxic (post-oxic) conditions. The key moment in this process is the deposition of chert prior to layer-silicate formation. The most probable phyllosilicate species in such an environment is berthierine, progressively transformed into chamosite during burial diagenesis. Other candidates, such as glauconite, illite or Fe-smectites, are less likely because of the thermodynamic

constraints (low pH and Eh and unsuitable ratios between the building elements) (Harder, 1974, 1978; Maynard, 1983).

The phyllosilicates from the hydrothermal-epigenetic facies of moderate-temperature (200–250°C) ore formation in the Kremikovtsi iron carbonate host show some specific features: crystalline and undeformed habits; relatively large particle size (no 'silt' fraction); low-temperature polytypes, low to no mixed layering, and a high degree of crystallinity; absence of impurities and dominant monomineralic aggregation; affiliation to initial open spaces and deposition mainly as vug fillings and linings. All these characteristics, demonstrating the authigenic nature of the hydrothermal layer silicates, imply that their mode of formation was under the pronounced control of initial vuggy porosity of the siderite host. This porosity probably originated after acid leaching of the carbonate medium due to aggressive hot hydrothermal fluids tracing pathways along the microtectonic framework.

In contrast, the dominant factor controlling hydrothermal deposition in silicate host rocks is the composition of the rock-forming minerals. They place 'advantageous for replacement structures' at the solution's disposal without complete dissolution and reprecipitation that generally gives more disparate mineralogical features than mentioned above. It is indicative that in the carbonate host, even replacement textures are not pseudomorphous but just crosscut siderite grains as a result of the extreme force of crystallization (Figure 5a).

There seems to be more of the phyllosilicate mineral variety at hydrothermal deposition sites in open spaces than the diagenetically induced phyllosilicate because of the neighboring stability fields of I-S, chamosite, berthierine and kaolinite under such conditions. The polytype variety at moderate temperatures (generally of dominant 1*M*-type) probably depends to a certain extent on the mineral-forming mechanism. The compositional variety allows us to distinguish them from low-temperature settings, thus emphasizing the specificity of hydrothermal layer-silicate formation in the carbonate host.

Berthierine as an indicator of geological setting

Genetic discriminations of clay minerals, and particularly of 14 Å chlorites and I-S, on the basis of their chemical composition have been performed by many authors (Albee, 1962; Foster, 1962; Kepezhinskas, 1965; Hower and Mowatt, 1966; Velde, 1985; Laird, 1988; Andreeva *et al.*, 1989; Drits and Kossowskaya, 1991, *etc.*). Some are given in this paper (Figures 4, 9, 10).

The absence of similar discrimination diagrams for berthierine may have been the result of its complicated diagnostics and because of terminological vagueness. As Slack *et al.* (1992) rightly noted, the difficulty in identifying berthierine by routine methods of mineralogical analysis suggests that much of the Fe-rich chlorite reported from modern and ancient massive sulfide deposits (but not only in this environment—present authors' addition) might actually be berthierine.

Toth and Fritz (1997) presented an excellent review of the data for berthierine occurrences, their geological setting, composition, forms and mineral associations. Adding their data to results from some other berthierine localities known from the literature, we made an attempt to look for a genetic relationship in compositional variations of this mineral. It can be seen in Figure 4a, b that berthierine compositions from genetically distinct geological settings are localized in relatively isolated fields. This difference, however, is better expressed on the plot in Figure 15. A similar diagram was used by Maynard (1986) to distinguish compositional relations of berthierine and chamosite in ironstones, but that author found no significant relationships. Comparison of the Al/Si *vs.* Mg/Fe ratios is very convenient because these pairs of elements are characterized by relatively close geochemical behavior in mineral systems related to isomorphic substitutions in each of the phases crystallized. Thus, these ratios reflect the initial geochemical relationships in solution/precursor and the conditions of mineral formation, *i.e.* the genetic affiliation of berthierine.

Three main genetic types of berthierine can be distinguished on the basis of its chemical composition: marine, non-marine and hydrothermal (Figure 15). The field of 'marine berthierine' comprises mainly its compositions in ironstones. They are scattered evenly around the average ratios of Al/Si = 1 (typical of kaolinite) and Mg/Fe = 0.25. Since the bulk of berthierine in ironstones is considered to be a transformation product of a kaolinite precursor (Bhattacharyya, 1983), the vertical variations are understandable. It is noteworthy that, as a rule, berthierine from hematitic ironstones is characterized by Al/Si $\geq$ 1 unlike minette ironstones with Al/Si $<$ 1. This is consistent with the Al/Si ratio of bulk ironstones from the first type which is almost twice as large as that from the second (recalculated data from James, 1966). Thus, the transformation mechanism of berthierine from a kaolinite precursor in ironstones probably involves complete dissolution-reprecipitation as proposed by Maynard (1986), and not a simple addition of bivalent cations (Fe^{2+} + Mg) to kaolinite and its structural reformation (*i.e.* a solid-state reaction).

The dashed line in Figure 15, partitioning four compositions of recent non-marine 'berthierines' from the bulk berthierine data, marks a particular field, named 'odinite'. This is because these "7-Å chamosites" (Porrenga, 1966; Rohrlich *et al.*, 1969) phases have subsequently been related to a distinct mineral species (Odin *et al.*, 1988), known by the name odinite (Bai-

ley, 1988c). Rude and Aller (1989) described ferric berthierine with small amounts of ^{IV}Al and a high occupancy of octahedral vacancies which should also be related to odinite. The other berthierine compositions included in this field are from ironstones and may include impurities of quartz and/or other phyllosilicates. The Mg/Fe ratios depend on the interrelation between Fe and Mg ions in the pore-water during diagenesis.

The field of 'non-marine berthierine' includes data for the mineral from various geological settings. It can be subdivided in two subgroups conventionally denoted as I and II. The dominant part of the reported compositions are aluminous with high Fe contents (subgroup non-marine I) whereas those from a deltaic/estuarine complex (Hornibrook and Longstaffe, 1996) are more siliceous and rich in Mg (non-marine II) (Figure 15). A plausible explanation for this difference may be the higher concentrations of Si and Mg in a delta/estuarine environment as a result of seawater input into the river delta/estuarine. It should be noted that although most berthierine from laterite/bauxite settings (non-marine I) is considered to have formed after replacement of a kaolinite precursor, it differs from the marine berthierines in its greater Al/Si ratio and smaller Mg contents. Thus, berthierine compositions depend less on the formation processes and more on the formation conditions (especially on ion-concentration ratios) of genetically distinct geological settings.

The 'hydrothermal berthierine' field is also subdivided into two subfields named (after Rusinova *et al.*, 1986) "pre-ore" (low temperature, in zones of hydrothermal alteration around ore deposits) and "ore" (high temperature, in orebodies). These two subfields are well differentiated on the diagram in Figure 15 as regards the Mg/Fe ratio which is greater in the pre-ore and less in the ore berthierines.

Another important feature of the ore berthierines (and associated 14 Å chlorites) in comparison with the pre-ore varieties is the greater Mn content, considered to be a mineralogical tracer implying the feeding channels of the hydrothermal ore-forming system (Rusinova *et al.*, 1986). The hydrothermal genetic type of berthierine includes data for the mineral from various ore deposits: volcanic-hosted Ag-polymetallic, polymetallic, Ag-Au epithermal, and Au-quartz vein deposits (Novak *et al.*, 1959; Rusinova *et al.*, 1986) as well as volcanogenic massive sulfide (Sudo, 1943; Slack *et al.*, 1992; Jiang *et al.*, 1992) and carbonate-hosted iron-barite-sulfide deposits of SEDEX type (this study). Thus, the berthierine composition can be an important mineralogical criterion in exploration work and mapping the ore deposit zoning.

It can be seen in Figure 15 that the two types of berthierine from the Kremikovtsi SIF belong to different fields (microcrystalline to the 'marine' one; radial bladed to the hydrothermal 'pre-ore' one), which is consistent with the petrographic observations mentioned in the previous section.

As noted by Brindley (1982) and Bailey (1988b), the monoclinic structural form is predominant in aluminous berthierines, a great many of which formed in bauxite/laterite geological settings (*i.e.* in a low-temperature environment). The lower aluminous varieties (assumed to be dominantly trigonal) are more characteristic of marine diagenetic and hydrothermal conditions. An impression is created that the relationship 'type of polytype-temperature of formation' is the same as in 14 Å chlorites: (1) *IIb* group (more ^{IV}Al) in medium-to-high temperature assemblages, the other groups (less ^{IV}Al)—in lower-temperature assemblages (Bailey and Brown, 1962); (2) a sequence of transformations in the structural groups of diagenetic chlorite in sediments as a function of depth of burial (Hayes, 1970); (3) pore-pressure and time being as important as temperature in controlling chlorite polytype occurrences (Walker, 1989). Harder (1978) noted, however, that low silica concentration in solution is the most important condition for low-temperature synthesis of berthierine. Rusinova *et al.* (1986) considered the solution composition and formation conditions, such as pH and f_{O_2}, to be leading factors controlling the compositions of hydrothermal berthierine. Thus, accepting berthierine chemistry as a key factor in determining its structural form, it should be concluded that the polytype variety of this mineral is a function, most of all, of the composition and concentration of building materials (soluble components or detrital clay particles), but not so much of the temperature of formation, pore-pressure, and time. Because berthierine generally occurred as a mixture of 1*T* and 1*M* polytypes, regardless of the geological setting (Brindley, 1982; Nikolskaya *et al.*, 1986), it seems likely that this is due to its metastable nature and especially to the local changes of the Al/Si and Fe/Si ratios and crystallization kinetics.

SUMMARY AND CONCLUSIONS

The features of layer silicates from the Kremikovtsi SEDEX SIF show that these minerals can be used as tracers to distinguish the two styles of mineralization (hydrothermal-sedimentary and hydrothermal-epigenetic) characteristic of this type of ore deposit.

The 'hydrothermal-sedimentary phyllosilicates' are minor minerals in the SIF. They are represented only by single findings of 'relict' Mg-rich berthierine and chamosite, analogous in composition and texture, formed as a transformation product after berthierine during progressive diagenesis. Generally, these Fe-Al layer silicates are microcrystalline to fine bladed, enriched in Mg, structurally imperfected, and associated in a typical diagenetic paragenesis (neomorphic siderite-berthierine/chamosite-framboidal/crystalline pyrite). The formation of berthierine can be linked to the

advanced stage of early diagenesis, immediately after chert deposition under anoxic conditions. The rarity of this mineral (and thus, of chamosite) in the hydrothermal-sedimentary facies is due to the abundant chert, the precipitation of which inhibits berthierine formation from hydrothermally modified seawater at low temperatures. A greater abundance of it in non- to low-chert SEDEX SIFs should be expected.

The 'hydrothermal-epigenetic phyllosilicates' (berthierine, chamosite, I-S, kaolinite) are better represented quantitatively in the Kremikovtsi SIF than the diagenetic ones. They have a series of specific characteristics: automorphic habits; large particle size atypical of phyllosilicates; perfect crystal structures; dominant 1*M* polytypes; relatively homogenous compositions; dominant monomineralic aggregates; open-space structures; association with barite and sulfides. The hydrothermal-epigenetic facies they included formed from acidic (pH = 3–5), hot (200–230°C), hydrothermal fluids invaded probably at the stage of burial diagenesis under relatively stable reducing conditions fluctuating near the sulfide/sulfate stability boundary.

Both types of phyllosilicates are precipitates from solution. Hydrothermal-sedimentary berthierine, however, did not have sufficient time under favorable conditions to crystallize perfectly and in abundance. It was confined, on the one hand, by the copious chert deposition, and on the other, by the progressive bacterial reduction of seawater sulfate, initiating immediate framboidal pyrite formation. In contrast, the hydrothermal-epigenetic assemblage is characterized mainly by stable crystal growth from saturated solution unloaded subsequently at the expense of its gradual alkalinity, ion-concentration changes, temperature decrease, and P_{O_2} fluctuations. The monostage hydrothermal deposition in open spaces within a carbonate host implies generally no dissolution-reprecipitation or replacement mechanisms of mineral formation, unlike in a silicate host.

The Al concentrations, greater in hydrothermal solutions than in seawater, explain the basic difference in phyllosilicate mineralogy of the Phanerozoic SEDEX and Precambrian cherty iron formations, which are dominated respectively by Fe-Al and by Fe (Al-free) species.

Berthierine, which is genetically a very important mineral not only for sedimentary iron ores, just like other layer silicates (chlorites, I-S), appears to be compositionally sensitive to formation conditions, thus indicating the geological setting in which it originated.

ACKNOWLEDGMENTS

We are particularly indebted to A. Ilieva for her advice and help with preparation of the samples for XRD studies, V. Dimov for TEM examinations, and M. Tarassov for his constructive comments on some thermodynamic interpretations and help during the microprobe studies (all from the Central Laboratory of Mineralogy and Crystallography, Bulgarian Academy of Sciences). The assistance of R. Mincheva (Central Laboratory of Mineralogy and Crystallography, Bulgarian Academy of Sciences) and M. Bechev (University of Mining and Geology, Sofia) in recording the XRD patterns is gratefully acknowledged. Thanks are due also to the management and staff of the Kremikovtsi open pit for their help during the regular field trips over the last 10 years. The authors thank the editors of *Clays and Clay Minerals* and two anonymous referees for the helpful and constructive reviews which led to significant improvements in the manuscript.

REFERENCES

Albee, A.L. (1962) Relationships between the mineral association, chemical composition and physical properties of the chlorite series. *American Mineralogist,* **47,** 851–870.

Alt, J.C. and Jiang, W.-T. (1991) Hydrothermally precipitated mixed-layer illite-smectite in recent massive sulfide deposits from the sea floor. *Geology,* **19,** 570–573.

Andreeva, O.V., Rusinova, O.V. and Volovikova, I.M. (1989) Typomorphic peculiarities of dioctahedral K-micas and mixed-layer formations from low-temperature wall-rock metasomatites. *Mineralogicheskii zhurnal,* **11,** 21–32 (in Russian, with English summary).

Arima, M., Fleet, M.E. and Barnett, R.L. (1985) Titanian berthierine: a Ti-rich serpentine-group mineral from the Picton ultramafic dyke, Ontario. *Canadian Mineralogist,* **23,** 213–220.

Bailey, S.W. (1988a) X-ray diffraction identification of the polytypes of mica, serpentine, and chlorite. *Clays and Clay Minerals,* **36,** 193–213.

Bailey, S.W. (1988b) Structures and compositions of other trioctahedral 1:1 phyllosilicates. Pp. 169–188 in: *Hydrous Phyllosilicates (Exclusive of Micas)* (S.W. Bailey, editor). *Reviews in Mineralogy,* **19**. Mineralogical Society of America, Washington, D.C.

Bailey, S.W. (1988c) Odinite, a new dioctahedral-trioctahedral Fe^{3+}-rich 1:1 clay mineral. *Clay Minerals,* **23,** 237–247.

Bailey, S.W. and Brown, B.E. (1962) Chlorite polytypism: I. Regular and semi-random one-layer structures. *American Mineralogist,* **47,** 819–850.

Bailey, S.W. and Tyler, S.A. (1960) Clay minerals associated with the Lake Superior iron ores. *Economic Geology,* **55,** 150–175.

Battaglia, S. (1999) Applying X-ray geothermometer diffraction to a chlorite. *Clays and Clay Minerals,* **47,** 54–63.

Bhattacharyya, D.P. (1983) Origin of berthierine in ironstones. *Clays and Clay Minerals,* **31,** 173–182.

Brindley, G.W. (1951) The crystal structure of some chamosite minerals. *Mineralogical Magazine,* **29,** 502–525.

Brindley, G.W. (1961) Kaolin, serpentine, and kindred minerals. Pp. 51–131 in: *The X-ray Identification and Crystal Structures of Clay Minerals* (G. Brown, editor). Mineralogical Society, London.

Brindley, G.W. (1982) Chemical compositions of berthierines—a review. *Clays and Clay Minerals,* **30,** 153–155.

Brindley, G.W. and Youell, R.F. (1953) Ferrous chamosite and ferric chamosite. *Mineralogical Magazine,* **30,** 57–70.

Brown, B.E. and Bailey, S.W. (1963) Chlorite polytypism. II. Crystal structure of a one-layer Cr-chlorite. *American Mineralogist,* **48,** 42–61.

Bubenicek, L. (1961) Recherches sur la constitution et la répartition des minerais de fer dans l'Aalénien de Lorraine. Thèse d'Ingénieur-Docteur, Faculté des Sciences de Nancy, 204 pp.

Curtis, C.D. and Spears, D.A. (1968) The formation of sedimentary iron minerals. *Economic Geology,* **63,** 257–270.

Curtis, C.D., Hughes, C.R., Whiteman, J.A. and Whittle, C.K. (1985) Compositional variation within some sedimentary chlorites and some comments on their origin. *Mineralogical Magazine,* **49,** 375–386.

Damyanov, Z.K. (1996) Genesis of the Kremikovtsi deposit and metallogenic perspectives of the Sredec iron ore region. *Geologica Balcanica,* **26,** 3–24.

Damyanov, Z.K. (1998) Ore petrology, whole-rock chemistry and zoning of the Kremikovtsi carbonate-hosted sedimentary exhalative iron(+Mn)-barite-sulfide deposit, Western Balkan, Bulgaria. *Neues Jahrbuch für Mineralogie Abhandlungen,* **174,** 1–42.

Deudon, M. (1955) La chamosite orthorhombique du minerai de Sainte-Barbe, couche grise. *Bulletin Société français de Minéralogie et de Cristallographie,* **78,** 475–480.

Deverin, L. (1945) *Étude pétrographique des minerais de fer oolithiques du Dogger des Alpes suisses.* Beitr. Geologie der Schweiz., Geotech. ser., Lf. **13**, v. 2, 115 pp.

Dickson, F.W. and Tunell, G. (1968) Mercury and antimony deposits associated with active hot springs in the western United States. Pp. 1673–1701 in: *Ore Deposits of the United States, 1933–1967,* Volume 2 (J.D. Ridge, editor). American Institute of Mining, Metallurgy and Petroleum Engineering.

Drits, V.A. and Kossowskaya, A.G. (1991) *Clay Minerals: Micas, Chlorites.* Nauka, Moscow 176 pp. (in Russian).

Drits, V.A., Plançon, A., Sakharov, B.A., Besson, G., Tsipursky, S.I. and Tchoubar, C. (1984) Diffraction effects calculated for structural models of K-saturated montmorillonite containing different types of defects. *Clay Minerals,* **19,** 541–561.

Eberl, D.D., Środoń, J., Lee, M., Nadeau, P.H. and Northrop, H.R. (1987) Sericite from the Silverton caldera, Colorado: Correlation among structure, composition, origin, and particle thickness. *American Mineralogist,* **72,** 914–934.

Ellis, A.J. (1967) The chemistry of some explored geothermal systems. Pp. 465–514 in: *Geochemistry of Hydrothermal Ore Deposits* (H.L. Barnes, editor). Holt, Rinehart and Winston, Inc., New York.

Emery, K.O., Hunt, J.M. and Hays, E.E. (1969) Thermal brines and ore sediments in the Red Sea: an overview. Pp. 557–571 in: *Hot Brines and Recent Heavy Metal Deposits in the Red Sea* (E.T. Degens and D.A. Ross, editors). Springer-Verlag, New York.

Engelhardt, W. von (1942) Die Strukturen von Thuringit, Bavalit und Chamosit und ihre Stellung in der Chlorit-gruppe. *Zeitschrift für Kristallographie,* **104,** 142–159.

Eugster, H.P. and Chou, I-M. (1973) The depositional environments of Precambrian banded iron-formations. *Economic Geology,* **68,** 1144–1168.

Floran, R.J. and Papike, J.J. (1975) Petrology of the low-grade rocks of the Gunflint iron-formation, Ontario-Minnesota. *Geological Society of America Bulletin,* **86,** 1169–1190.

Foster, M.D. (1962) Interpretation of the composition and a classification of the chlorites. *U.S. Geological Survey Professional Paper*, **414-A**, 33 pp.

Halbach, P. (1970) Mineral constituents and facies development of the principal seam horizon of the Franconian Dogger beta in the area of the claim of the "Kleiner Johannes" company near Pegnitz, Upper Franconia. *Geologische Jahrbuch,* **88,** 471–507.

Hallimond, A.F. (1939) On the relation of chamosite and daphnite to the chlorite group. *Mineralogical Magazine,* **25,** 441–465.

Harder, H. (1974) Illite mineral synthesis at surface temperatures. *Chemical Geology,* **14,** 241–253.

Harder, H. (1978) Synthesis of iron layer silicate minerals under natural conditions. *Clays and Clay Minerals,* **26,** 65–72.

Hayes, J.B. (1970) Polytypism of chlorite in sedimentary rocks. *Clays and Clay Minerals,* **18,** 285–306.

Hornibrook, E.R.C. and Longstaffe, F.J. (1996) Berthierine from the Lower Cretaceous Clearwater Formation, Alberta, Canada. *Clays and Clay Minerals,* **44,** 1–21.

Horton, D.G. (1983) Argillic alteration associated with the Amethyst vein system, Creede mining district, Colorado. Ph.D. thesis, University of Illinois, Urbana, Illinois.

Hower, J. and Mowatt, T.C. (1966) The mineralogy of illites and mixed-layer illite/montmorillonites. *American Mineralogist,* **51,** 825–854.

Hughes, C.R. (1987) The composition and origin of layer silicates in iron-formations and ironstones: a preliminary analytical transmission electron microscopical study. Ph.D. thesis, University of Sheffield, UK.

Iijima, A. and Matsumoto, R. (1982) Berthierine and chamosite in coal measures of Japan. *Clays and Clay Minerals,* **30,** 264–274.

Inoue, A. and Utada, M. (1983) Further investigations of a conversion series of dioctahedral mica/smectites in the Shinzan hydrothermal alteration area, northeast Japan. *Clays and Clay Minerals,* **31,** 401–412.

James, H.L. (1954) Sedimentary facies of iron-formation. *Economic Geology,* **49,** 235–293.

James, H.L. (1966) Chemistry of the iron-rich sedimentary rocks. *US Geological Survey Professional Paper*, **440-W,** 61 pp.

Jiang, W.-T., Peacor, D.R. and Slack, J.F. (1992) Microstructures, mixed layering, and polymorphism of chlorite and retrograde berthierine in the Kidd Creek massive sulfide deposit, Ontario. *Clays and Clay Minerals,* **40,** 501–514.

Kalaydzhiev, S. (1982) New data on the structure of Kremikovtsi Ore Field. *Review of the Bulgarian Geological Society,* **43,** 159–171 (in Bulgarian with English abstract).

Kalgeropoulos, S.I. and Scott, S.D. (1985) Mineralogy and geochemistry of tuffaceous exhalites (Tetsusekiei) of the Fukazawa mine, Hokuroku district, Japan. Pp. 412–432 in: *The Kuroko and Related Volcanogenic Massive Sulfide Deposits* (B.J. Skinner, editor). *Economic Geology,* Monograph, **5**.

Kastner, M. (1979) Silica polymorphs. Pp. 99–109 in: *Marine Minerals* (R.G. Burns, editor). Reviews in Mineralogy, **6**. Mineralogical Society of America, Washington, D.C.

Keller, W.D. (1988) Authigenic kaolinite and dickite associated with metal sulfides—probable indicators of a regional thermal event. *Clays and Clay Minerals,* **36,** 153–158.

Kepezhinskas, K.B. (1965) *Statistical Analysis of Chlorites and their Paragenetic Types.* Nauka, Moscow, 135 pp. (in Russian).

Kimberley, M.M. (1989) Exhalative origins of iron formations. *Ore Geology Reviews,* **5,** 13–145.

Klekl, L.V. (1979) Regularities of chamosite distribution in bauxites of the Belgorod District of the Kursk magnetic anomaly. *Lithology and Mineral Resources,* **14,** 377–382 (in Russian).

Kodama, H. and Foscolos, A.E. (1981) Occurrence of berthierine in Canadian Arctic desert soils. *Canadian Mineralogist,* **19,** 279–283.

Kotelnikov, D.D. and Konyukhov, A.I. (1986) *Clay Minerals in Sedimentary Rocks.* Nedra, Moscow, 247 pp. (in Russian).

Laird, J. (1988) Chlorites: metamorphic petrology. Pp. 405–453 in: *Hydrous Phyllosilicates (Exclusive of Micas)* (S.W. Bailey, editor). Reviews in Mineralogy, **19**. Mineralogical Society of America, Washington, D.C.

Lu, G., McCabe, C., Henry, D.J. and Schedl, A. (1994) Origin of hematite carrying a Late Paleozoic remagnetization in a quartz sandstone bed from the Silurian Rose Hill Formation, Virginia, USA. *Earth and Planetary Science Letters,* **126,** 235–246.

MacGregor, M., Lee, G.W. and Wilson, G.V. (1920) *The Iron Ores of Scotland.* British Geological Survey Memoir Special Reports on Mineral Resources, **11,** 240 pp.

Maxwell, D.T. and Hower, J. (1967) High-grade diagenesis and low-grade metamorphism of illite in the Precambrian Belt series. *American Mineralogist,* **52,** 843–857.

Maynard, J.B. (1983) *Geochemistry of Sedimentary Ore Deposits.* Springer-Verlag, New York, 305 pp.

Maynard, J.B. (1986) Geochemistry of oolitic iron ores, an electron microprobe study. *Economic Geology,* **81,** 1473–1483.

McDowell, S.D. and Elders, W.A. (1980) Authigenic layer silicate minerals in borehole Elmore 1, Salton Sea geothermal field, California, USA. *Contributions to Mineralogy and Petrology,* **74,** 293–310.

Nemecz, E. (1981) *Clay Minerals.* Akadémiai Kiadó, Budapest, 547 pp.

Nikolskaya, N.K., Goilo, E.A. and Frank-Kamenetsky, V.A. (1986) X-ray diffraction peculiarities of disordered one-layer orthogonal berthierine. *Mineralogicheskii zhurnal,* **8,** 89–93 (in Russian with English summary).

Novák, F., Vtelensky, J., Losert, J., Kupka, F. and Valcha, Z. (1959) Orthochamosit, ein neues Mineral aus den hydrothermalen Erzgängen von Kank bei Kutná Hora (Kuttenberg) in der Tschechoslowakei. *Geologie,* **8,** 159–167.

Odin, G.S., Bailey, S.W., Amouric, M., Fröhlich, F. and Waychunas, G.A. (1988) Mineralogy of the verdine facies. Pp. 159–206 in: *Green Marine Clays* (G.S. Odin, editor). Developments in Sedimentology, **45.** Elsevier, Amsterdam.

Omelyanenko, B.I., Volovikova, I.M., Drits, V.A., Zvyagin, B.B., Andreeva, O.V. and Sakharov, B.A. (1982) On the content of term sericite. *Izvestiya Akademii Nauk SSSR, seriya Geologicheskaya,* **5,** 69–87 (in Russian).

Panayotov, V. (1974) The Kremikovtsi iron ore deposit. Pp. 257–266 in: *Twelve Ore Deposits in Bulgaria* (P. Dragov and B. Kolkovski, editors). 4th IAGOD Symposium, Varna, Publishing House of the Bulgarian Academy of Science, Sofia.

Perelman, A.I. (1989) *Geochemistry.* Vysshaya shkola, Moscow, 528 pp. (in Russian).

Popov, P. (1989) Tectonic position and structures of the Upper Cretaceous mineralizations in Banat-Srednogorie and Western Balkan metallogenic zones, Bulgaria. Dr.Sci. thesis, University of Mining & Geology, Sofia, 543 pp. (in Bulgarian).

Porrenga, D.H. (1966) Clay minerals in recent sediments of the Niger delta. Pp. 221–233 in: *Clays and Clay Minerals, Proceedings of the 14th National Conference* (S.W. Bailey, editor). Pergamon Press, New York.

Protich, M. (1955) Étude minéralogique des phyllites de quelques minerais de fer de Serbie (Yougoslavie). *Bulletin Société français de Minéralogie et de Cristallographie,* **78,** 528–534.

Rohrlich, V., Price, N.B. and Calvert, S.E. (1969) Chamosite in the recent sediments of Loch Etive, Scotland. *Journal of Sedimentary Petrology,* **39,** 624–631.

Rude, P.D. and Aller, R.C. (1989) Early diagenetic alteration of lateritic particle coatings in Amazon continental shelf sediments. *Journal of Sedimentary Petrology,* **59,** 704–716.

Rusinova, O.V. and Rusinov, V.L. (1980) Structural features of chlorites from epithermal ore deposits. Pp. 281–291 in: *Scientific Bases and Utilization of the Typomorphism of Minerals.* Proceedings of the XI IMA meeting, Novosibirsk. Nauka, Moscow (in Russian with English abstract).

Rusinova, O.V. and Rusinov, V.L. (1986) Compositional variations, polytypism, and formation conditions of dioctahedral K-micas. Pp. 41–59 in: *Metasomatism, Mineralogy, and Genetic Questions of Volcanic-Hosted Gold and Silver Deposits* (D.S. Korzhinskii, editor). Nauka, Moscow (in Russian).

Rusinova, O.V., Rusinov, V.L. and Troneva, N.V. (1986) Composition, some structural features, and formation conditions of wall-rock alteration and ore chlorites and berthierines. Pp. 5–40 in: *Metasomatism, Mineralogy, and Genetic Questions of Volcanic-Hosted Gold and Silver Deposits* (D.S. Korzhinskii, editor). Nauka, Moscow (in Russian).

Schultz, R.W. (1966) Lower Carboniferous cherty ironstones at Tynagh, Ireland. *Economic Geology,* **61,** 311–342.

Shilin, A.V., Kotelnikov, D.D., Solodkova, N.A. and Vachugova, L.I. (1979) On the diagnostics and genesis of chamosite in ancient sedimentary rocks. *Vestnik Moskovskogo Universiteta, seriya Geologiya,* **4,** 49–58 (in Russian).

Slack, J.F., Jiang, W.-T., Peacor, D.R. and Okita, P.M. (1992) Hydrothermal and metamorphic berthierine from the Kidd Creek volcanogenic massive sulfide deposit, Timmins, Ontario. *Canadian Mineralogist,* **30,** 1127–1142.

Środoń, J. and Eberl, D.D. (1984) Illite. Pp. 495–544 in: *Micas* (S.W. Bailey, editor). Reviews in Mineralogy, **13.** Mineralogical Society of America, Washington, D.C.

Sudo, T. (1943) On some low temperature hydrous silicates found in Japan. *Bulletin of the Chemical Society of Japan,* **18,** 281–329.

Sudo, T. and Shimoda, S. (1978) *Clays and Clay Minerals of Japan.* Elsevier, Amsterdam, 326 pp.

Taylor, K.G. (1990) Berthierine from the non-marine Wealden (Early Cretaceous) sediments of south-east England. *Clay Minerals,* **25,** 391–399.

Thurrell, R.G., Sergeant, G.A. and Young, B.R. (1970) *Chamosite in Weald Clay from Horsham, Sussex.* Natural Environmental Research Council, Report 70/7.

Toth, T.A. and Fritz, S.J. (1997) An Fe-berthierine from a Cretaceous laterite: Part I. Characterization. *Clays and Clay Minerals,* **45,** 564–579.

Tronkov, D. and Damyanov, Z. (1993) Triassic fossil remains in the siderite ore of the Kremikovtsi iron ore deposit. *Geologica Balcanica,* **23,** 34.

Tvaltschrelidze, A.G. and Scheglov, V.I. (1990) A mineralogical-geochemical model of vein barite ore-genesis. *Zapiski Vsesoyuznogo Mineralogicheskogo Obshchestva,* **119,** 21–34 (in Russian, with English abstract).

Tyler, S.A. and Bailey, S.W. (1961) Secondary glauconite in the Biwabic iron-formation of Minnesota. *Economic Geology,* **56,** 1033–1044.

Vassileff, L. (1993) Pre-Late Cretaceous collides in Bulgaria. *Review of the Bulgarian Geological Society,* **54,** 1–19 (in Bulgarian with English abstract).

Velde, B. (1985) *Clay Minerals. A Physico-Chemical Explanation of their Occurrence.* Developments in Sedimentology, **40,** Elsevier, Amsterdam, 427 pp.

Velde, B., Raoult, J.-F. and Leikine, M. (1974) Metamorphosed berthierine pellets in Mid-Cretaceous rocks from north-eastern Algeria. *Journal of Sedimentary Petrology,* **44,** 1275–1280.

Walker, J.R. (1989) Polytypism of chlorite in very low grade metamorphic rocks. *American Mineralogist,* **74,** 738–743.

Walker, J.R. (1993) Chlorite polytype geothermometry. *Clays and Clay Minerals,* **41,** 260–267.

Warren, E.A. and Curtis, C.D. (1989) The chemical composition of authigenic illite within two sandstone reservoirs as analysed by ATEM. *Clay Minerals,* **24,** 137–156.

Weiss, Z. and Durovic, S. (1983) Chlorite polytypism. II. Classification and X-ray identification of trioctahedral polytypes. *Acta Crystallographica,* **B39,** 552–557.

Weissberg, B.G., Browne, P.L. and Seward, T.M. (1979) Ore metals in active geothermal systems. Pp. 738–780 in: *Geochemistry of Hydrothermal Ore Deposits,* 2nd edition (H.L. Barnes, editor). John Wiley & Sons, New York.

White, D.E. (1967) Mercury and base-metal deposits associated with thermal mineral waters. Pp. 575–631 in: *Geochemistry of Hydrothermal Ore Deposits* (H.L. Barnes, editor). Holt, Rinehart and Winston, Inc., New York.

White, S.H., Huggett, J.M. and Shaw, H.F. (1985) Electron-optical studies of phyllosilicate intergrowths in sedimentary and metamorphic rocks. *Mineralogical Magazine,* **49,** 413–423.

Yau, Y.-C., Peacor, D.R., Beane, R.E., Essene, E.J. and McDowell, S.D. (1988) Microstructures, formation mechanisms, and depth-zoning of phyllosilicates in geothermally altered shales, Salton Sea, California. *Clays and Clay Minerals,* **36,** 1–10.

Yershova, Z.P., Nikitina, A.P., Perfilev, Y.D. and Babeshkin, A.M. (1976) Study of chamosites by gamma-resonance (Mössbauer) spectroscopy. Pp. 211–219 in: *Proceedings of the International Clay Conference, 1975, Mexico City* (S.W. Bailey, editor). Applied Publishing, Wilmette, Illinois.

Zhabin, A.G., Samsonova, N.S. and Isakovich, I.Z. (1987) *Mineralogical Studies of Wall-rock Alteration Halos.* Nedra, Moscow, 159 pp. (in Russian).

E-mail of corresponding author: zdamyanov@mail.bg

(Received 19 December 1999; revised 17 April 2001; Ms. 410; A.E. Richard L. Hay)